THE INFLUENCES OF STRESS AND TEMPERATURE UPON THE TIME TO INITIATE PLASTIC DEFORMATION IN AN ANNEALED LOW CARBON STEEL

Thesis by

David S. Wood

In Partial Fulfillment of the Requirements

For the Degree of

Doctor of Philosophy

California Institute of Technology

Pasadena, California

1949

ACKNOWLEDGMENTS

The author wishes to express his grateful appreciation to Professor Donald S. Clark, who directed this research, and whose aid and encouragement made the work possible. Throughout the course of the research, many valuable comments and suggestions were made by Professor Pol E. Duwez. Professor A. Hollander contributed helpful criticism of the design of the rapid load testing machine. Mr. Thad Vreeland aided greatly in the performance of the tests and in the preparation of the figures.

The rapid load testing machine was constructed under a contract with the Air Materiel Command, United States Air Force, and the testing program was carried out under a contract with the Office of Naval Research, United States Navy. Thanks are expressed to both of these agencies for their sponsorship of the work.

ABSTRACT

An experimental investigation of the time delay for initiation of plastic deformation in an annealed low carbon steel is described. The delay time is determined as a function of the applied stress at temperatures of -75°F, 73°F, 150°F, and 250°F. The stress is applied in a continuous manner within a period of about 7 millisec, and the stress is maintained substantially constant thereafter, until plastic deformation begins. At any given temperature, the relation between the logarithm of the delay time and the stress is found to consist of two straight lines which join together at a point in the delay time-stress plane. One is a line of constant stress, and the other is a line along which the logarithm of the delay time decreases linearly as the stress is increased above the constant stress line. The experimental results are compared with a dislocation theory of yielding in low carbon steel which has been given by A. H. Cottrell and B. A. Bilby (21)*. It is shown that this theory, in its present form, does not describe the experimental results adequately. Two suggestions are made for modification and addition to the theory which might lead to satisfactory agreement with the experimental observations.

---

* The figures appearing in parentheses refer to the references listed at the end of this thesis.

TABLE OF CONTENTS

TABLE OF CONTENTS (continued)

LIST OF TABLES

LIST OF FIGURES

LIST OF FIGURES (continued)

I. INTRODUCTION

Considerable thought and experimental investigation has been devoted to the study of the mechanical properties of metals and alloys under conditions of dynamic loading. The effects of rate of loading and rate of deformation upon the uniaxial stress-strain relation have been investigated extensively in recent years (1-7). In the range of plastic deformations, it is found that the stress at a given strain is increased when the rate of loading or rate of deformation is increased. For the majority of metals and alloys the effect is apparently comparatively small, not exceeding about 50 per cent increase in stress, even at the rates of loading and deformation encountered in high speed impact tests. Duwez and Clark (8) performed impact tests on annealed copper, cold rolled mild steel, and annealed aluminum. They found that the plastic deformation waves which are propagated from the impacted end of long wires and rods of these materials may be predicted quite closely from the static stress-strain relations by using von Kármán's theory (9,10) for the propagation of plastic deformation in solids.

However, a notable exception to this observation occurs in the behavior of annealed low carbon steels. This material is distinguished from the other common metals and alloys by the fact that it exhibits a well defined upper yield stress. The upper yield stress coincides with the elastic limit. Several investigators have studied the effects of the rate of application

of load upon the upper yield stress and other features of the stress-strain curves of such steels. Some studies which have been made at moderate rates, such as can be obtained in conventional testing machines, are those of Elam (11), Davis (12), Winlock and Leiter (13,14), and Miklowitz (15). All of these investigators found that the upper yield stress of annealed low carbon steels was quite markedly increased by increased rate of loading or rate of extension. As an example Miklowitz tested a 0.02 per cent carbon steel in the form of flat bars which had a uniform gage section 1.5 in. long. He found that the upper yield stress increased from 35,300 lb/in.^{2} at a head speed of 2.56×10^{-2} in./min to 49,500 lb/in.^{2} at a head speed of 15.4 in./min.

Much greater effects have been observed in impact experiments. As early as 1905 Bertram Hopkinson (16) performed impact experiments on long wires. He was primarily interested in studying the elastic waves produced by the impact of falling weights. However, in the course of the investigation he noticed that an annealed iron wire having a static upper yield stress of 40,000 lb/in.^{2} could withstand a stress exceeding 75,000 lb/in.^{2} for a time of the order of one millisec, without detectable permanent deformation.

This result has been confirmed by the more recent results of Duwez and Clark (8). They performed tension impact tests on 80 in. long wires and compression tests on 12 in. long rods of annealed low carbon steels. In these test one end of the wire or rod was subjected to an impact by a hammer moving with a known velocity. If the bar remains elastic the

amplitude of the stress wave which is initiated at the impacted end is given by

$$\sigma = \frac{v}{c_o} E;$$

where σ is the stress, v is the velocity of impact, c_o is the wave velocity, and E is Young's modulus. By determining the maximum impact velocity for which the bar remains elastic the upper yield stress may be found using the relation given above. In this way Duwez and Clark found that the upper yield stress in tension, of wires having a static upper yield stress of 24,600 lb/in.^{2}, was 72,000 lb/in.^{2} under impact conditions. From the compression impact tests a dynamic upper yield of 90,000 lb/in.^{2} was found for rods having a static upper yield stress of 42,000 lb/in.^{2}

Thus for annealed low carbon steel, stresses of from 2 to 3 times the static upper yield stress may be sustained for a time of the order of one millisec without causing permanent deformation.

Recently a new experimental technique has been developed by Professor Donald S. Clark and the author which is particularly suited for the determination of the length of time during which a material may behave elastically at stresses in excess of the static elastic limit. This technique and some experimental results which have been obtained are described in a paper (17) to be published. In this method a constant tensile stress is applied to a specimen and the deformation is measured as a function of time. The stress is increased from zero to its final value in a continuous manner within a total time of about 10 millisec. It is then held constant for the remainder of the test. The test specimen is short enough and the

rate of rise of stress low enough so that no appreciable stress waves occur in the specimen.

Using this type of loading, tests were made on a 0.19 per cent carbon annealed steel. The results showed that a well defined period of time was required for the initiation of plastic deformation at stresses exceeding the static upper yield stress. This delay time was found to vary continuously from 5 millisec at a stress of about 51,000 lb/in.^{2} to 6 sec at a stress of about 37,000 lb/in.^{2} The static upper yield stress of the material was 36,000 lb/in.^{2} Tests were also made on three alloy steels and two aluminum alloys. None of these materials exhibited a definite delay time for the initiation of plastic deformation.

The purpose of the present investigation is to obtain experimental evidence which will aid in determining the nature of the mechanism for the initiation of plastic deformation in annealed low carbon steel. The method used is to investigate the dependence of the delay time upon temperature as well as stress. In this way the effect of thermal activation upon the mechanism may be quantitatively determined. Before describing the experiments and results of this investigation, some experimental and theoretical studies made by other investigators concerning the mechanical properties of low carbon steel will be discussed. These studies bear some relation to the results obtained in the present investigation.

The tensile or compressive stress-strain relation for annealed low carbon steel is distinguished from those of the other common metals and alloys by the presence of a definite

yield point. That is, the transition from elastic to plastic behavior is abrupt rather than continuous. Immediately after plastic deformation has begun the stress which the material will sustain is less than the upper yield stress. The initial portion of the plastic deformation takes place at a substantially constant stress which is called the lower yield stress. The amount of plastic deformation which takes place at the lower yield stress is known as the yield strain. The magnitude of the yield strain is a few per cent for the common low carbon steels at ordinary temperatures. For strains greater than the yield strain the material strain hardens in the same manner as other metals and alloys.

Another phenomenon exhibited by low carbon steels which is either absent or much less pronounced in other materials is known as strain ageing. If a low carbon steel is deformed plastically, followed by removal of the load, and aged for a sufficient length of time, then upon re-loading it is found that the material exhibits a new upper yield stress. The ageing time required decreases as the ageing temperature is increased.

It has been shown by at least three investigators (18-20) that the yield point is associated with the presence of small quantities of carbon or nitrogen, of the order of 0.001 per cent. Low and Gensamer (20) showed this by treating the material in wet hydrogen at 720°C for a sufficient period to remove all of the carbon and nitrogen. Static tensile tests made on the material so treated did not exhibit a definite yield point. When either carbon or nitrogen was reintroduced

separately by suitable carburizing or nitriding treatment the definite yield point returned. Strain ageing was found to be removed and returned by the same treatment.

Recently Cottrell and Bilby (21) have presented a theory for the yield point and strain ageing of iron. This theory is based upon the inhibition of the motion of dislocations by the interstitially dissolved carbon or nitrogen atoms. Since these foreign atoms relieve hydrostatic tension stress in the dilated portion of the dislocation field, an interaction energy with the dislocation is produced which leads to an attractive force. Thus the interstitially dissolved foreign atoms migrate by thermal diffusion to preferred positions in the dislocation field, forming an "atmosphere" around the dislocation. In the dilated portion of the field the concentration is greater than the average concentration in the material, while in the compressed portion it is less. The quantity of carbon atoms required to form saturated "atmospheres" around all of the dislocations in the undeformed material is of the order of 0.001 per cent.

Due to such "atmospheres" the dislocations lie in potential wells. Therefore they cannot move freely when external stresses are applied to the material. If a sufficiently high stress is applied a dislocation may be separated from its "atmosphere." The separation process is governed by thermal activation. The activation energy is a function of the applied stress, and Cottrell and Bilby have made an approximate computation of the form of this function. After the dislocation has been separated from its "atmosphere" it moves under a smaller exter-

nal stress than the stress required for the separation process. Thus such a mechanism offers a possible basis for an explanation of the upper and lower yield stresses in low carbon steel. Also, according to this theory, the thermal activation of the separation process leads to a mean time to separate a dislocation from its "atmosphere." Hence the theory affords a basis for an understanding of the time delay for the initiation of plastic deformation. However, it is not clear how the separation of individual dislocations is connected with the initiation of macroscopically observable plastic deformation.

Cottrell and Bilby have also shown that strain ageing may be understood on the basis of their theory of the interaction of interstitially dissolved carbon and nitrogen with dislocations. After some plastic deformation of the material, some dislocations are in regions of only normal concentration of foreign atoms. If the material is aged for a sufficient time, "atmospheres" reform around these dislocations by thermal diffusion of the foreign atoms. Hence the yield point will return. Some of the details of this theory are presented below in the discussion of the results of the present investigation.

II. EQUIPMENT

The principal equipment used in this investigation may be listed as follows.

A. A rapid load tensile testing machine of special design was used to apply the loads to the test specimens. This machine is hydro-pneumatically operated. It is capable of applying any desired load up to a maximum of 10,000 lb within a period of time of about 7 millisec. A cutaway perspective drawing of the machine is shown in Fig. 1, and a section drawing is shown in Fig. 2. These figures show the machine as originally constructed. For the present investigation the two columns which support the upper or stationary head were replaced by longer columns. This provides the additional space required for the apparatus used to control the temperature of the specimen.

B. A specimen heat exchanger, shown in the section drawing in Fig. 3, was used as a means for controlling the temperature of the specimen. It forms a jacket around the specimen through which suitable heated or cooled fluids are circulated.

C. A dynamometer, shown in Fig. 3, was used to detect the load acting on the specimen. The dynamometer is of the resistance sensitive wire strain gage type.

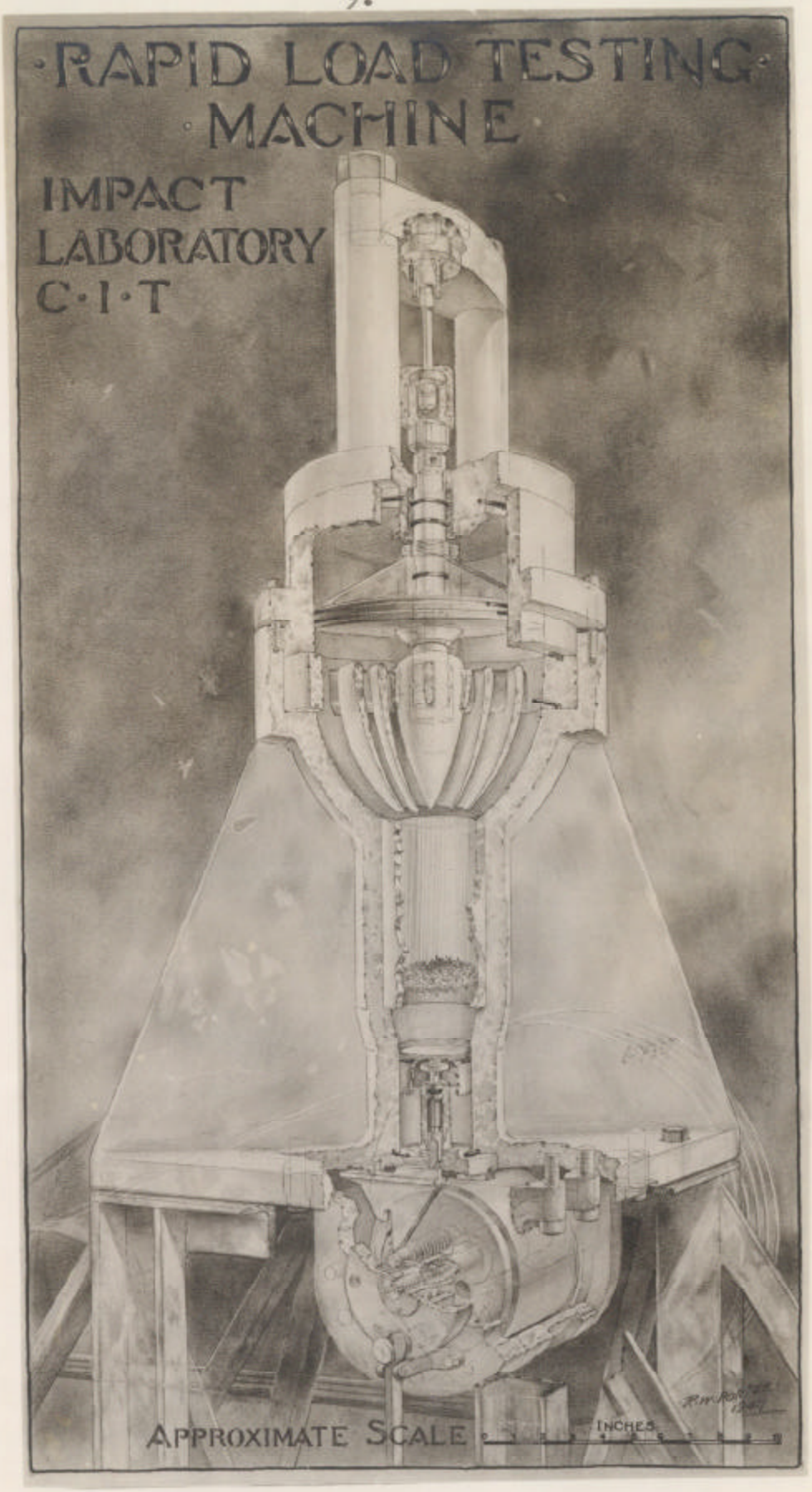

Fig. 1 Rapid Load Testing Machine

Fig 2 Section Drawing Testing Machine

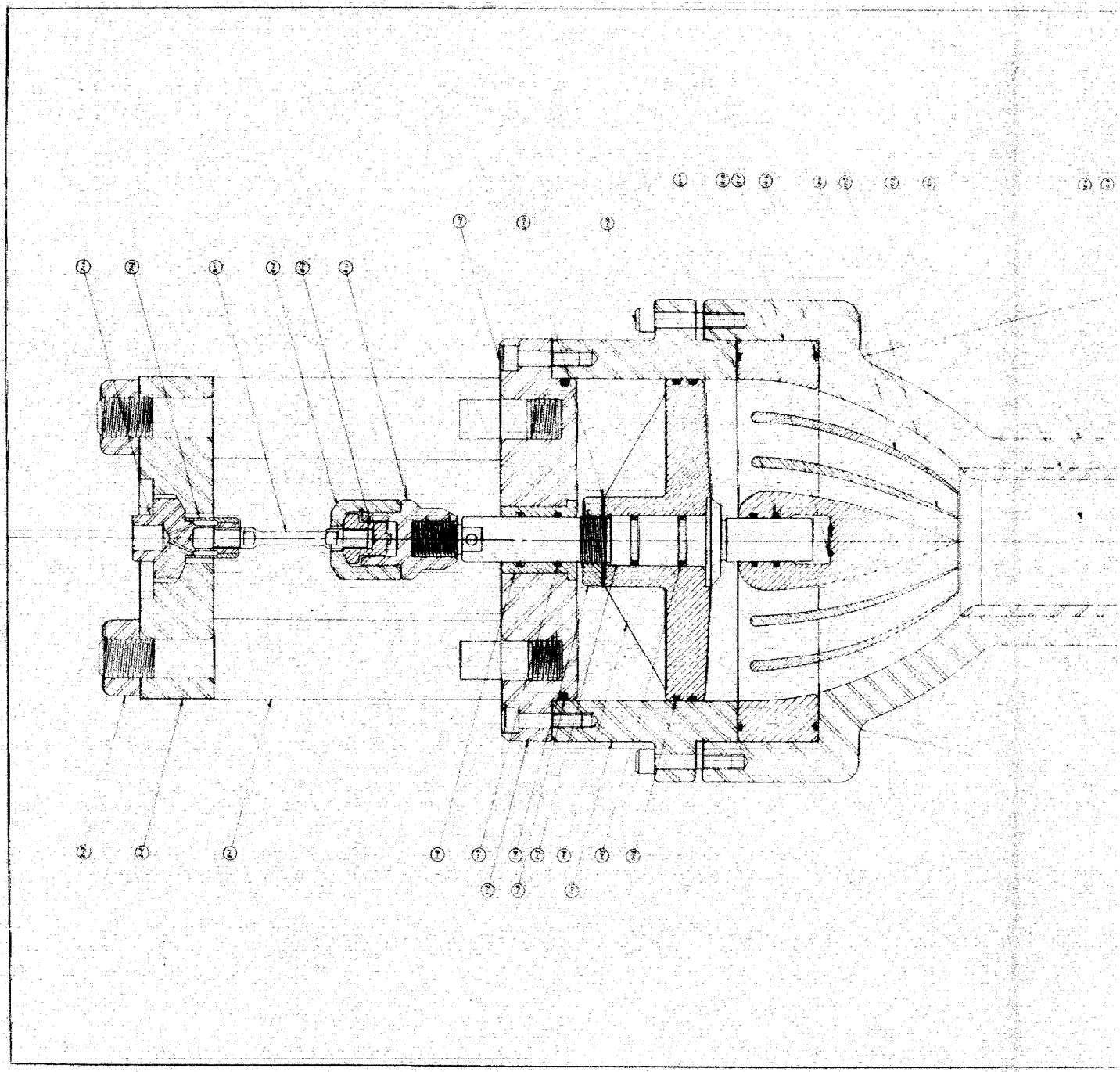

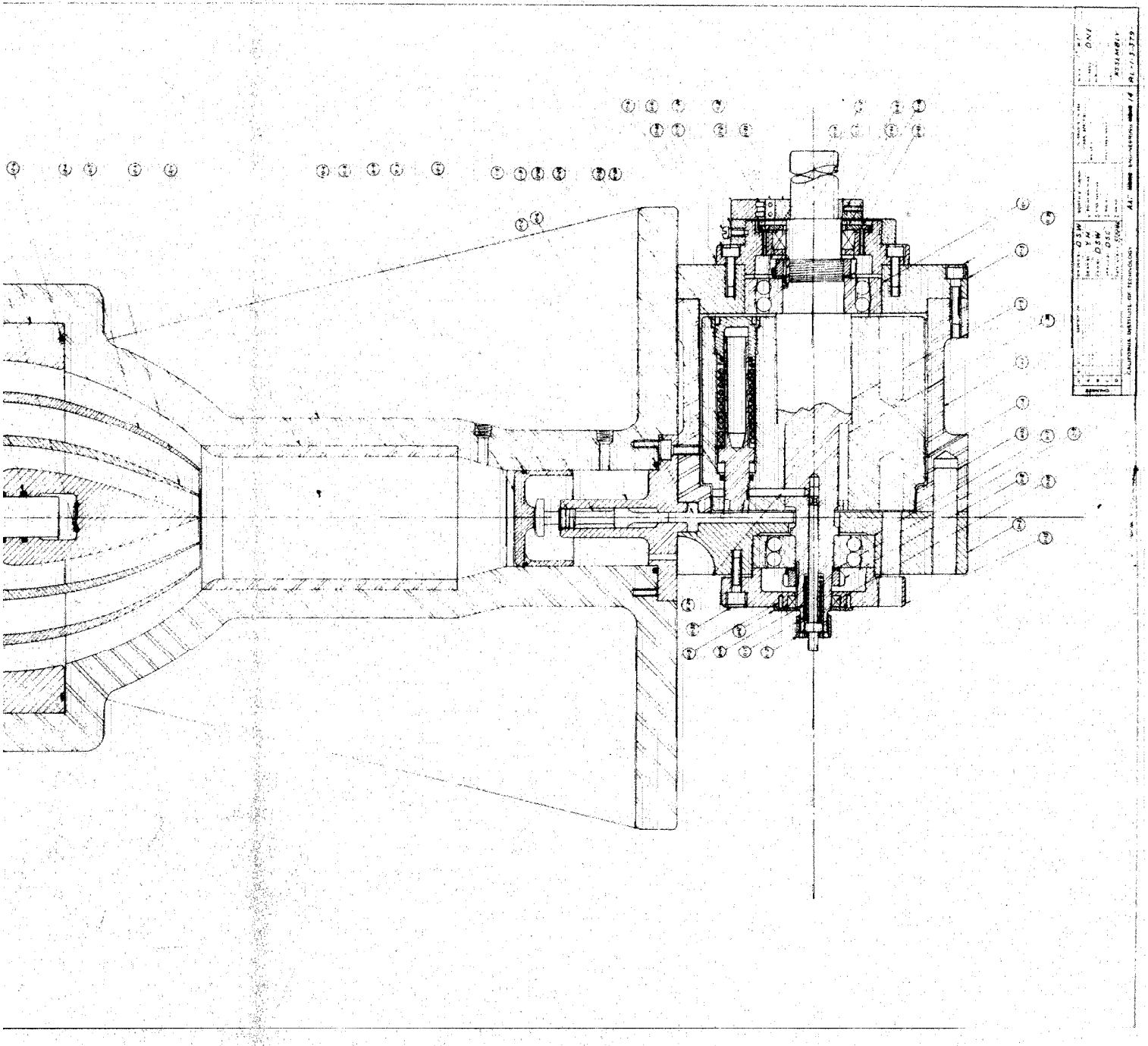

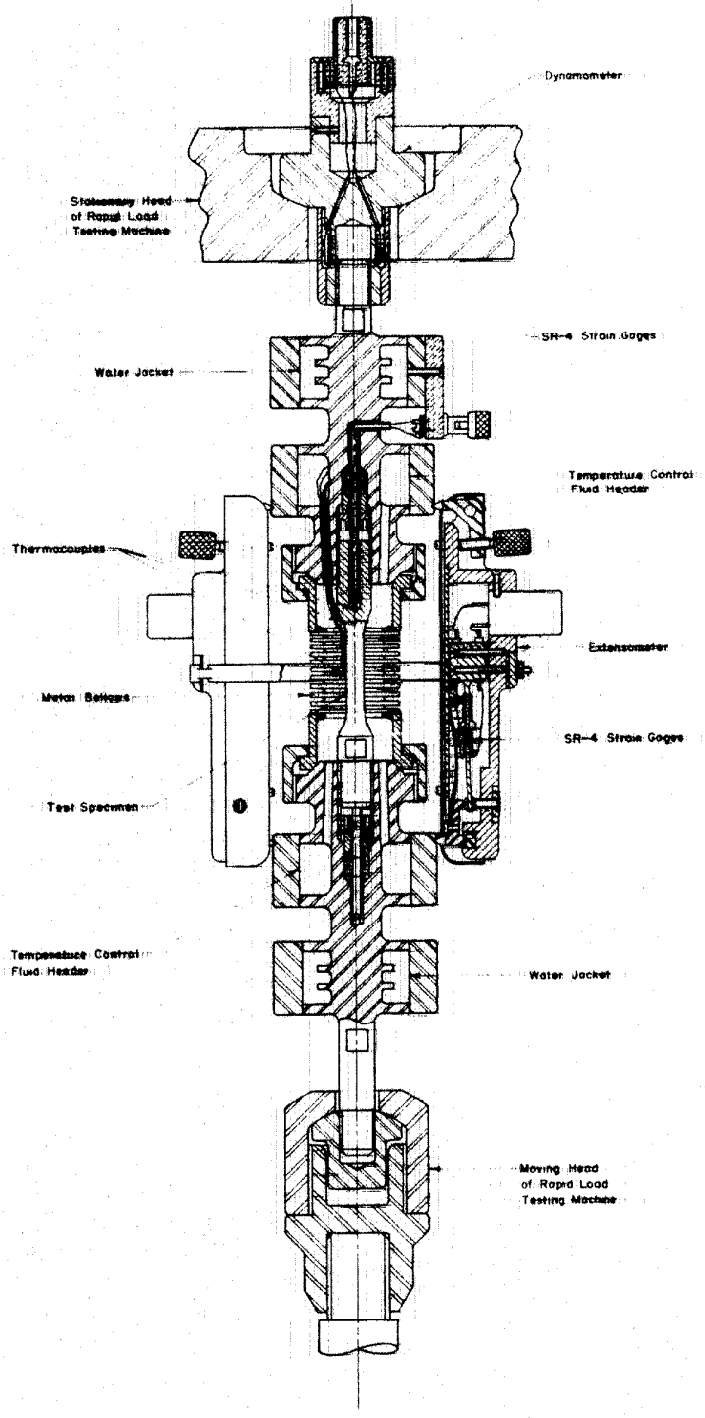

Fig. 3 Arrangement for Controlled Temperature Tests in Rapid Load Testing Machine

D. An extensometer, shown in Fig. 3, was used to detect the extension of the specimen. It is also of the resistance sensitive wire strain gage type.

E. A recording unit, shown in the photograph in Fig. 4, was used to record the signals from the dynamometer and extensometer. Suitable electronic and photographic means are employed in this unit.

F. An alcohol cooling and circulating unit, shown in the foreground of the photograph in Fig. 5, was used to cool alcohol and circulate it through the specimen heat exchanger. The alcohol is cooled by solid carbon dioxide. A centrifugal pump provides the means for circulation of the alcohol through the specimen heat exchanger.

G. An oil heating and circulating unit, shown in Fig. 6, was used to heat oil and circulate it through the specimen heat exchanger. The oil is heated by an electric immersion heater. A gear pump is used to circulate the oil through the specimen heat exchanger.

H. Static test equipment, consisting of a 30,000 lb Riehle testing machine and suitable extensometers, was used to determine the static stress-strain relation of the steel employed in this investigation at several temperatures.

Fig.4 Recording Unit

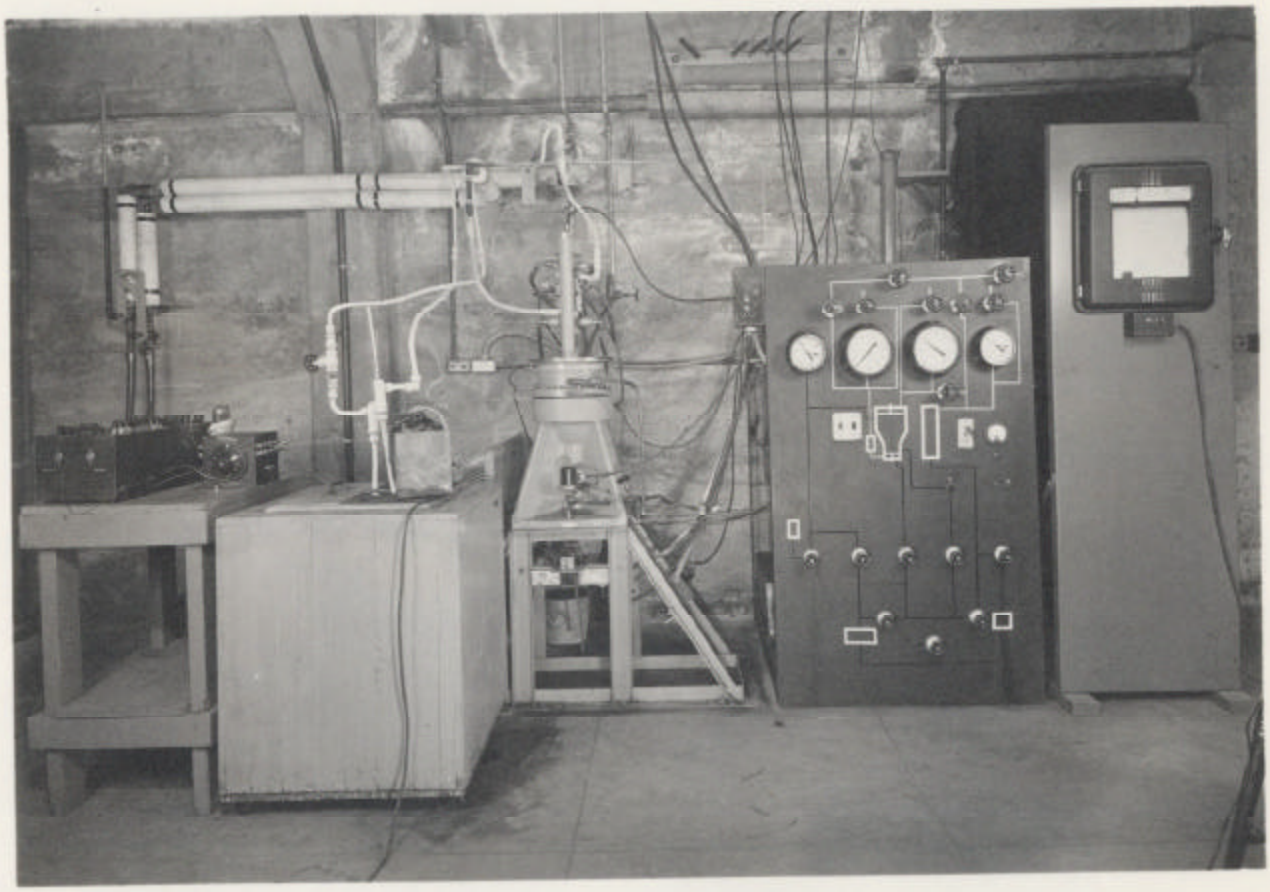

Fig.5 General View of Equipment

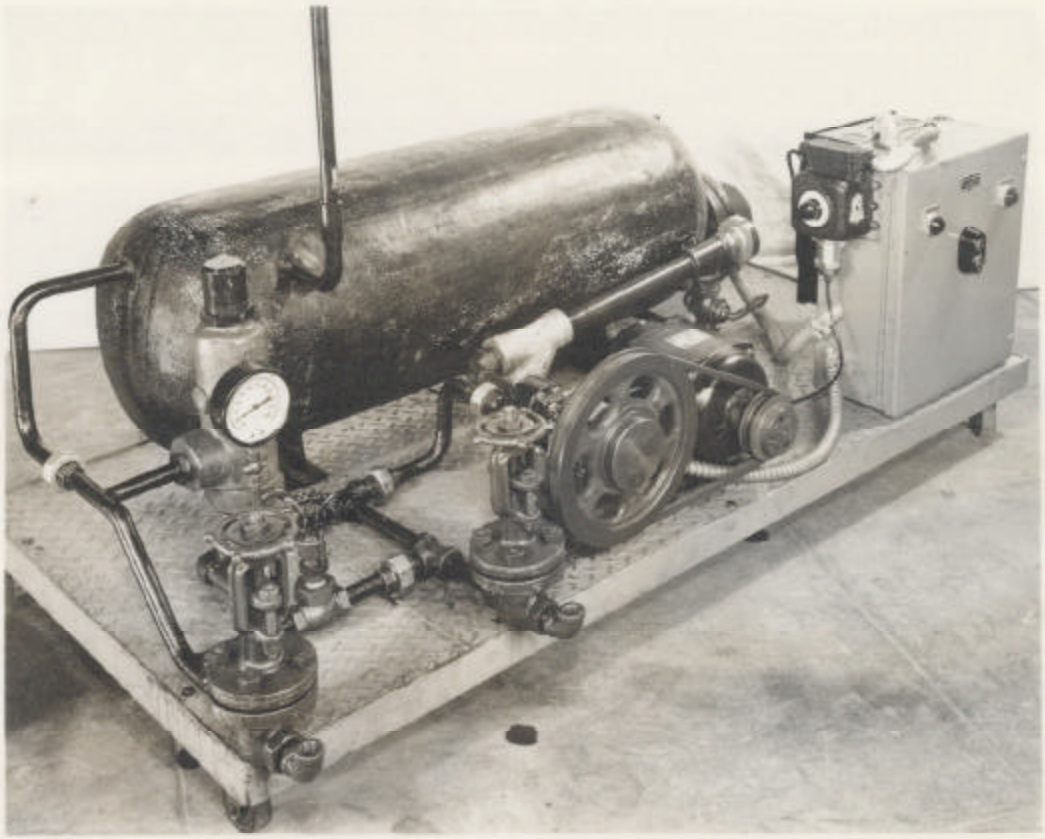

Fig.6 Oil Heating and Circulating Unit

I. Temperature measurement equipment, consisting of copper-constantan thermocouples and a Leeds and Northrup portable precision potentiometer, was used to measure the temperature of the specimen.

A photograph showing a general view of the equipment is presented in Fig. 5. A photograph showing the specimen heat exchanger and extensometer in operation in the rapid load testing machine is presented in Fig. 7.

The rapid load testing machine, dynamometer, and recording equipment, designed by the author, have been described by Professor Donald S. Clark and the author in a report (22) to the U. S. Air Force, Air Materiel Command, and in a paper (17) to be published by the American Society for Testing Materials. Since neither of these references is readily available at the present time, this equipment together with the additions and modifications made for the present investigation will be described in detail.

A. Rapid Load Testing Machine

The machine is designed to apply a tensile load in as short a time as possible and in such a way that the stress is substantially uniform throughout the gage length of the specimen at any given instant. The load-time relation consists of a continuous increase of load over a short finite period of time, followed by a period of indefinite length during which the load remains constant at the maximum value attained during the test. The length of the specimen is short enough and the rate of rise of load low enough so that the stress at any given instant is uniform over the gage length of the specimen to a

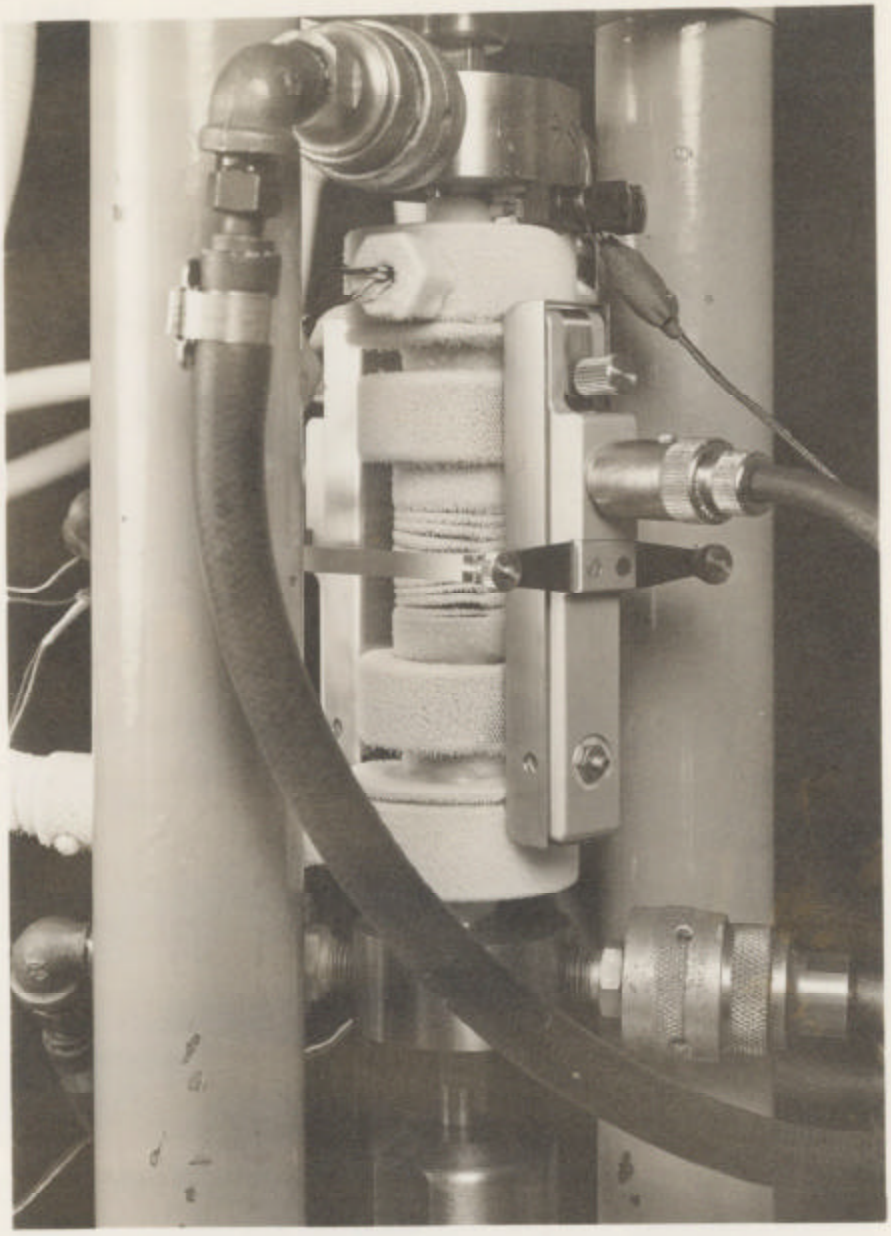

Fig.7 Specimen Heat Exchanger and Extensometer in Operation

close approximation. The term "rapid loading" has been used by Clark and the author to distinguish this type of loading from impact loading. In the latter case the stress distribution is not uniform along the gage length of the specimen.

A simple mechanical arrangement which produces a load-time relation of the desired form is a critically damped vibratory system having one degree of freedom. If the mass of such a system is subjected to a step function force, the force in the spring increases in a continuous manner and approaches the applied force in minimum of time without overshooting. Critical damping is obtained when

$$C = 2\sqrt{KM}\,, \tag{1}$$

where C is the coefficient of viscous damping,

K is the spring constant, and

M is the mass of the system.

If a force, Fo, is suddenly applied to the mass at the time t = o, then the force, F, in the spring is given by

$$F = F_o\left[1-\left(1+\frac{t}{\alpha}\right)e^{-t/\alpha}\right], \tag{2}$$

where

$$\alpha = \sqrt{\frac{M}{K}}\,, \tag{3}$$

and e is the base of natural logarithms. Since the spring force, F, approaches the applied force, Fo, asymptotically it is desirable to adopt some convention to specify the total rise time, T. One such convention is the time between the intersections of the maximum slope tangent to the curve of F vs. t given by equation (2) with the coordinate lines F = 0 and F = Fo. It can be shown that this time is given by

$$T = e\alpha\,. \tag{4}$$

The rapid load testing machine is designed to approximate the simple system discussed above, with the test specimen forming a part of the spring. Referring to Figs. 1, 2, and 3, the machine is constructed as follows. The ends of the specimen heat exchanger are threaded to fit the force measuring unit, or dynamometer, and the lower or moving head of the machine. The dynamometer rests in a spherical seat in a fixed cross head at the top of the machine, and the cross head is supported by two heavy columns. The lower head includes a second spherical seat, and threads onto the upper end of the main piston rod of the machine.

The piston rod passes through a central hole in the top head into the pressure cylinder, and is sealed by two rubber "O" rings. The lower end of the piston rod is guided in the hub of the vane system, and sealed by two "O" rings. The small space in the hub below the rod is vented to atmosphere by a central hole in the piston rod. The loading piston, rigidly attached to the piston rod, fits closely in the cylinder and carries two "O" ring seals. The load is applied to the specimen by means of air pressure in the closed chamber above the piston. The chamber below the loading piston, extending down to the actuating piston, is completely filled with a glycerine-water mixture. Immediately below the loading piston is the vane system consisting of a central hub and two circumferential guide vanes rigidly attached to an outer annular ring by six spokes.

The cylindrical section below the vane system contains the damping unit, and the actuating piston. The damping unit

consists of a close-packed arrangement of tubes, each with an inside diameter of 0.079 in., a wall thickness of 0.008 in., and a length of 6 in. This nest of tubes is contained in a sleeve, and the assembly of tubes and sleeve is brazed together to form an integral unit. The tube nest provides viscous damping of the system, which may be adjusted by varying the viscosity of the fluid. The theory of the design of the damping unit is discussed later.

The actuating unit consists of a small piston below the damping unit, a plunger, and a sliding cam operated by a rotating mechanism. The piston, sealed against the walls of the small cylinder by a single "O" ring, is supported on a suitably guided plunger. The lower end of the plunger rests on the top surface of the sliding cam. During a test, the cam is moved along horizontal ways by an actuating pin in the rotating mechanism. The top surface of the cam has two levels connected by a linearly sloping surface. During the horizontal motion of the cam, the lower end of the plunger follows the sloping cam surface, thus allowing the actuating piston to move downward under the action of the fluid pressure. As the actuating piston moves downward, the fluid pressure on the lower side of the loading piston progressively decreases. A constant air pressure is maintained above the loading piston. Hence the specimen is loaded as the actuating piston moves downward. A relatively low positive air pressure is applied to the chamber below the actuating piston. This serves to maintain sufficient positive pressure on the fluid above the actuating piston during the loading cycle to prevent cavitation.

The actuating pin lies in a hole in one face of the solid steel rotor, parallel to the rotor axis and eccentric to it. This pin is urged outward by a heavy spring to a position in which it engages the cam. It may be held in the retracted position by the trigger pin located radially in the rotor. The trigger pin is held in place by the trigger bar located axially in and protruding from the end of the rotor shaft. The trigger bar is reduced in section near the point at which it supports the trigger pin, so that if the trigger bar is moved inward the trigger pin drops into the reduced section of the trigger bar thus releasing the actuating pin. The aptuating pin then moves rapidly outward to its working position. The movement of the trigger bar required for triggering the machine is provided by the plunger of a solenoid (not shown in Figs. 1 and 2) which strikes the end of the trigger bar when the solenoid is energized. The solenoid coil is connected in series with a commutator type contact mounted on the opposite end of the rotor shaft. The contact provides for triggering when the rotor is in such a position that approximately 3/4 of a revolution is required before the actuating pin contacts the cam. Thus the maximum available time is allowed for the actuating pin to reach its working position. The cam and actuating pin are arranged so that the engagement of the pin with the vertical surface of the cam occurs when the pin is moving nearly tangential to the cam surface. This insures smooth motion of the cam and minimizes dynamic stresses in the various parts.

One end of the rotor shaft of the actuating unit is

provided with a multiple "V" belt sheave, driven from a jack shaft. The jack shaft is fitted with two fly wheels and is driven by a direct current electric motor. A wide range of speed is obtained by varying the armature voltage supply to the motor. The purpose of the fly wheels is to provide sufficient energy in the drive system at the lower speeds so that the speed will not be decreased by the sliding friction forces acting on the cam.

The rate of loading of the specimen is controlled by means of the actuating unit and the drive unit. For a given slope of cam the rate of loading is proportional to the rotor speed. The cam velocity at constant rotor speed is sinusoidal with time. However, the sloping surface of the cam passes under the plunger of the actuating unit when the actuating pin is in its topmost position. Hence, the cam speed is practically constant for the relatively short distance of cam travel during which the loading occurs.

The maximum extension to which a specimen may be subjected by the machine is 0.05 in., because the height of the step on the cam is 0.5 in. and the ratio of the area of the loading piston to that of the actuating piston is 10:1.

The manipulation of the testing machine is accomplished by means of a control system which contains the necessary valves, pressure gages, vacuum pump, fluid pump, and reservoirs arranged for convenient operation. The operating panel of the control system may be seen in the photograph in Fig. 5 to the right of the testing machine.

In order to analyze quantitatively the operating

characteristics of a machine of the type outlined above, the following idealizations and assumptions are made. The specimen, specimen heat exchanger and the members of the machine which carry the load are considered as a linearly elastic spring whose stiffness may be computed from the dimensions and arrangement of the parts. Attached to this spring is the loading piston which is considered to move without friction in its cylinder. A constant air pressure is maintained on the specimen side of the piston. The fluid occupying the space between the loading and actuating pistons is assumed to be incompressible, and the walls of the fluid chamber to be infinitely rigid. Also the fluid flow is assumed to be laminar (viscous) everywhere; that is, the Reynold's number is below the critical value. The pressure drop across the damping unit is assumed to be directly proportional to the rate of flow through it. The actuating piston moves without friction in its cylinder. Furthermore, it is assumed that the time required for strain waves to travel through the specimen and its supports and the time for pressure waves to travel through the fluid are small compared with the minimum time of rise of load on the specimen.

The limiting case for the minimum time for the increase of the load on the specimen is that in which the actuating piston is instantaneously released and allowed to move freely under the action of the fluid pressure. If the machine is constructed such that a minimum time of rise of load is obtained without oscillation for this mode of operation, then the machine will have the optimum design for following

faithfully any desired controlled motion applied to the actuating piston by means of a cam or otherwise.

The idealized machine and the notation is presented in Fig. 8. The value of the damping coefficient, C, is determined by the diameter and length of the tubes in the damping unit, the fluid viscosity, and the area of the large piston and the area of the tube nest. C is a constant only if certain conditions regarding the size of the tubes are fulfilled. These conditions and the evaluation of C are given below. For the present, it is necessary only to assume that C is a constant.

The equation of motion of the large piston and the fluid moving with it is given by

$$m_1 \frac{d^2x}{dt^2} + Kx = (p_0 - p_1)A_1 . \qquad (5)$$

The equation of motion of the small piston and the fluid moving with it is given by

$$m_2 \frac{A_1}{A_2} \frac{d^2x}{dt^2} = (p_2 - p_3) A_2 . \qquad (6)$$

These two equations are related by the pressure drop across the damping unit as given by the definition of C, namely,

$$(p_1 - p_2) = \frac{C}{A_1} \frac{dx}{dt} . \qquad (7)$$

Combining these three equations, the following relation is obtained:

$$\left[m_1 + m_2 \left(\frac{A_1}{A_2}\right)^2\right] \frac{d^2x}{dt^2} + C \frac{dx}{dt} + Kx = (p_0 - p_3)A_1, \qquad (8)$$

which describes the motion of the system. For convenience the following two quantities may be defined:

$M = \left[m_1 + m_2 \left(\frac{A_1}{A_2}\right)^2\right]$ is the equivalent mass of the system;

$F_0 = (p_0 - p_3) A_1$ is the final load on the specimen;

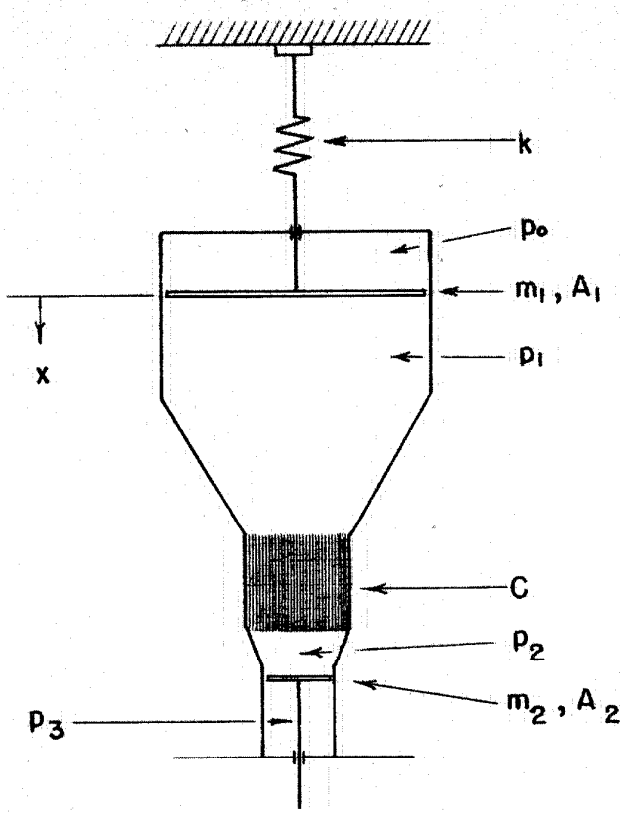

x = Displacement of loading piston, in.
t = Time, sec.
k = Stiffness of the machine, lb/in.
m_1 = Mass of loading piston and that portion of the fluid that moves at the piston velocity, lb sec^2/in.
m_2 = Mass of actuating piston and that portion of the fluid that moves at the piston velocity, lb sec^2/in.
A_1 = Area of loading piston, in^2
A_2 = Area of actuating piston, in^2
p_o Constant pressure above loading piston, lb/in^2
p_1 = Fluid pressure between loading piston and damping unit, lb/in^2
p_2 = Fluid pressure immediately above actuating piston, lb/in^2
p_3 = Constant pressure below actuating piston, lb/in^2
C = Damping coefficient defined by $A_1(p_1 - p_2) = C\, dx/dt$, lb sec/in.

Fig.8 Idealized Testing Machine

so the equation of motion becomes

$$M\frac{d^2x}{dt^2} + C\frac{dx}{dt} + Kx = F_o. \qquad (9)$$

This is the usual equation for a simple spring-mass system with viscous damping subjected to a suddenly applied disturbing force. Its solution for the case of critical damping is given in equations 1, 2, and 3 above.

The determination of the numerical values of the equivalent mass, M, and the spring constant, K, from the dimensions of the machine is straightforward. However the determination of a numerical value for the viscous damping coefficient, C, requires further consideration. By equation (7)

$$C = \frac{pA_1}{dx/dt},$$

where the pressure drop across the damping unit, $p_1 - p_2$, has been replaced by p. Also, $\frac{dx}{dt}$, the velocity of the loading piston, is $\frac{dx}{dt} = \frac{A}{A_1} V_o$, where V_o is the average fluid velocity in the damping unit for steady state flow, and A is the total cross-sectional area of the tubes. The pressure drop, p, across the damping unit for steady state viscous flow is given by the usual relation

$$p = 8\frac{L\mu}{r_o^2} V_o, \qquad (9)$$

where L = Length of tubes,

μ = absolute viscosity of fluid,

and r_o = radius of a tube.

Using these relations, C becomes

$$C = 8\frac{L\mu}{r_o^2}\frac{A_1^2}{A}. \qquad (10)$$

It is to be noted that the pressure drop given by equation (9) applies only to steady flow conditions. During

the time of rise of load in the machine, the flow is certainly not steady, since the fluid velocity, V, varies from zero to a maximum and back to zero in that time. However, it can be shown that if the tubes are small enough, steady state flow conditions will be established in a time that is short compared to the characteristic rise time, T.

To show this the pressure drop under conditions of varying viscous flow is examined. Although the actual flow and pressure in the damping tubes of the rapid load machine are rather complicated functions of time, sufficient information may be obtained by considering a relatively simple case. Namely the case of a circular pipe suddenly subjected to a pressure difference from end to end, with this pressure difference maintained constant after its application.

To facilitate the mathematical treatment, the following assumptions are made.

1. The pipe is straight and of a constant circular cross-section.
2. The stream lines are straight and parallel to the pipe axis. If the pipe is many diameters long, the end effects which are neglected by this assumption will be negligibly small.
3. The fluid is incompressible.

The boundary conditions to be satisfied by the solution are as follows.

1. The velocity is zero at the wall of the pipe at all times.
2. The velocity is zero at all points at the time t=0.

3. At the time t = 0, a pressure difference, p, is applied between the ends of the pipe, and is constant thereafter.

The two independent variables are taken as

t = time, measured from the instant of pressure application, and r = radius, measured from the pipe center line.

The dependent variable is taken as

v = velocity of fluid as a function of r and t.

The notation for the other physical quantities involved is as follows:

r_o = inner radius of the pipe,

L = length of the pipe,

P = pressure difference between the ends of the pipe,

ρ = density of the fluid, and

μ = absolute viscosity of the fluid.

The equation of motion is obtained by considering a hollow cylindrical element of fluid of radius, r, thickness, dr, and length, L. The velocity gradients on the inner and outer surface of the element are as shown in the accompanying sketch so that the viscous friction force on the element becomes,

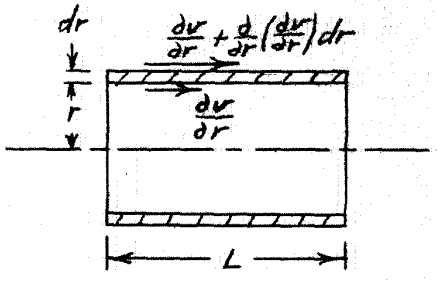

$$2\pi(r+dr)L\mu\left[\frac{\partial v}{\partial r} + \frac{\partial^2 v}{\partial r^2}dr\right] - 2\pi r L\mu\frac{\partial v}{\partial r}$$

$$= 2\pi L\mu\left[r\frac{\partial^2 v}{\partial r^2} + \frac{\partial v}{\partial r}\right]dr,$$

neglecting terms of the order $(dr)^2$. The force on the element due to the applied pressure is 2π rpdr, the mass is $2\pi rL\rho\,dr$, and the acceleration is $\frac{\partial v}{\partial t}$, so that the equation of motion

becomes

$$\frac{\partial v}{\partial t} - \frac{\mu}{\rho}\left[\frac{\partial^2 v}{\partial r^2} + \frac{1}{r}\frac{\partial v}{\partial r}\right] = \frac{p}{L\rho}. \qquad (11)$$

Equation (11) is solved by the usual method of finding the general solution for the equation with the right hand side set equal to zero and adding to it a particular solution for the complete equation.

For the general solution of

$$\frac{\partial v}{\partial t} - \frac{\mu}{\rho}\left[\frac{\partial^2 v}{\partial r^2} + \frac{1}{r}\frac{\partial v}{\partial r}\right] = 0 \qquad (12)$$

the variables are separated by setting $v = R(r) \times T(t)$, where $R(r)$ is a function of r only, and $T(t)$ is a function of t only. Upon substitution in equation (12), the relation

$$\frac{T'}{T} = \frac{\mu}{\rho}\left[\frac{R''}{R} + \frac{1}{r}\frac{R'}{R}\right]$$

is obtained, where the primes indicate differentiation of the functions T and R with respect to their single variables.

Thus $\frac{T'}{T} = \kappa$,

whose solution is $T = T_0 e^{\kappa t}$,

and $R'' + \frac{1}{r}R' - \kappa\frac{\rho}{\mu}R = 0$,

where κ and T_0 are arbitrary constants. The latter is a form of Bessel's differential equation whose general solution in terms of Bessel functions of the first and second kinds is

$$R(r) = C_1 J_0\left(\sqrt{-\kappa\tfrac{\rho}{\mu}}\, r\right) + C_2 Y_0\left(\sqrt{-\kappa\tfrac{\rho}{\mu}}\, r\right).$$

However, since $Y_0(0) = -\infty$ and v must be finite at $r = 0$, then $C_2 = 0$, leaving one arbitrary constant, C_1. Therefore, the solution of equation (12) is

$$v = C e^{\kappa t} J_0\left(\sqrt{-\kappa\tfrac{\rho}{\mu}}\, r\right).$$

Since κ is arbitrary, any number of such solutions may be added to obtain a general solution of equation (12) in the

form of an infinite series, namely,

$$v = \sum_{\kappa} C_\kappa e^{\kappa t} J_0\left(\sqrt{-\kappa \frac{\rho}{\mu}}\, r\right). \tag{13}$$

For the required particular solution of equation (11), take $v = P(r)$, a function of r only. Substituting in equation (11), it is observed that P(r) must satisfy the relation

$$P'' + \frac{1}{r} P' = -\frac{p}{L\mu}.$$

This may be rewritten as

$$\frac{1}{r} \frac{d}{dr}\left(r \frac{dP}{dr}\right) = -\frac{p}{L\mu},$$

and by direct integration the solution is

$$P(r) = -\frac{p}{4L\mu} r^2 + D_1 \log r + D_2. \tag{14}$$

But again, since v must be finite at $r = 0$, $D_1 = 0$.

Adding equations (13) and (14), the general solution of equation (11) is

$$v = \sum_{\kappa} C_\kappa e^{\kappa t} J_0\left(\sqrt{-\kappa \frac{\rho}{\mu}}\, r\right) - \frac{p}{4L\mu} r^2 + D_2. \tag{15}$$

Applying boundary condition (1):

$$0 = \sum_{\kappa} C_\kappa e^{\kappa t} J_0\left(\sqrt{-\kappa \frac{\rho}{\mu}}\, r_0\right) - \frac{p}{4L\mu} r_0^2 + D_2.$$

From this it is apparent that $J_0\left(\sqrt{-\kappa \frac{\rho}{\mu}}\, r_0\right)$ must be zero for all values of κ. This requires that $\sqrt{-\kappa \frac{\rho}{\mu}}\, r_0 = \gamma_n$, where γ_n is a positive root of J_0, and n indicates the number of the roots in ascending order of magnitude. Thus κ is determined by

$$\kappa = -\gamma_n^2 \frac{\mu}{\rho r_0^2}.$$

Also, from this boundary condition

$$D_2 = \frac{p}{4L\mu} r_0^2.$$

Using these values of κ and D_2 and applying boundary condition (2),

$$0 = \sum_{n=1}^{\infty} C_n J_0\left(\gamma_n \frac{r}{r_0}\right) + \frac{p}{4L\mu}\left(r_0^2 - r^2\right).$$

This condition serves to determine the coefficients C_n , as follows. Expand the term $\frac{pr_o^2}{4L\mu}\left\{1-\left(\frac{r}{r_o}\right)^2\right\}$ in a Fourier-Bessel series

$$f(x)=\sum_{n=1}^{\infty} a_n J_o(\gamma_n x) \quad , \quad 0\le x\le 1,$$

where f(x) is a function subject to certain restrictions which are satisfied by $\left\{1-\left(\frac{r}{r_o}\right)^2\right\}$, and the coefficients a_n are given by

$$a_n = \frac{2}{J_1^2(\gamma_n)} \int_o^1 t\, f(t) J_o(\gamma_n t)\, dt .$$

In this case, put $x=\frac{r}{r_o}$, so f(x) becomes

$$\frac{pr_o^2}{4L\mu}\left\{1-\left(\frac{r}{r_o}\right)^2\right\} = \sum_{n=1}^{\infty} a_n J_o\left(\gamma_n \frac{r}{r_o}\right),$$

with

$$a_n = \frac{2}{J_1^2(\gamma_n)} \int_o^1 t\, \frac{pr_o^2}{4L\mu}\left\{1-t^2\right\} J_o(\gamma_n t)\, dt.$$

The latter integral may be evaluated by integration by parts and use of the recurrence relations for Bessel functions, and is found to be

$$a_n = \frac{pr_o^2}{L\mu} \frac{J_2(\gamma_n)}{\gamma_n^2 J_1^2(\gamma_n)} .$$

Therefore, the boundary condition (2) becomes

$$0=\sum_{n=1}^{\infty} C_n J_o\left(\gamma_n \frac{r}{r_o}\right) + \sum_{n=1}^{\infty} \frac{pr_o^2}{L\mu} \frac{J_2(\gamma_n)}{\gamma_n^2 J_1^2(\gamma_n)} J_o\left(\gamma_n \frac{r}{r_o}\right).$$

This equation may be satisfied term by term by putting

$$C_n = -\frac{pr_o^2}{L\mu} \frac{J_2(\gamma_n)}{\gamma_n^2 J_1^2(\gamma_n)} ,$$

which may be simplified by using the recurrence relation

$$J_o(\gamma_n) + J_2(\gamma_n) = \frac{2}{\gamma_n} J_1(\gamma_n).$$

But $J_o(\gamma_n)=0$, since γ_n is a root of J_o . Consequently C_n becomes

$$C_n = -\frac{pr_o^2}{L\mu} \frac{2}{\gamma_n^3 J_1(\gamma_n)} .$$

Substituting all of these results in equation (15), the final solution adapted to the boundary conditions is

$$v = \frac{pr_o^2}{4L\mu}\left[\left\{1-\left(\frac{r}{r_o}\right)^2\right\} - 8\sum_{n=1}^{\infty} e^{-\gamma_n^2 \frac{\mu}{\rho r_o^2} t} \frac{J_o\left(\gamma_n \frac{r}{r_o}\right)}{\gamma_n^3 J_1(\gamma_n)}\right]. \qquad (16)$$

For purposes of numerical representation of the solution, two parameters of the system are defined. First,

$$V_o = \frac{p r_o^2}{8 L \mu}$$

is the average velocity of the fluid in the steady state. Second,

$$\tau = \frac{\rho r_o^2}{\mu} \tag{17}$$

has the dimensions of time and is the time constant for reaching steady state flow. With these parameters, equation (16) becomes

$$\frac{v}{V_o} = 2\left[\left\{1-\left(\frac{r}{r_o}\right)^2\right\} - 8\sum_{n=1}^{\infty} e^{-\gamma_n^2 t/\tau} \frac{J_o(\gamma_n \frac{r}{r_o})}{\gamma_n^3 J_1(\gamma_n)}\right]. \tag{18}$$

The series in this equation converges quite rapidly, and velocity profiles in dimensionless form $\left(\frac{v}{V_o} \text{ vs. } \frac{r}{r_o}\right)$ are plotted in Fig. 9 for three intermediate values of the time parameter, t/τ, and for the steady state flow, $t/\tau = \infty$.

The average velocity, V, may be defined by

$$V = \frac{2}{r_o^2}\int_o^{r_o} v\, r\, dr .$$

If the value of v given by equation (18) is substituted in the above equation, V is obtained as a function of time, namely

$$V = \frac{2}{r_o^2} 2V_o\left[\int_o^{r_o} r\left\{1-\left(\frac{r}{r_o}\right)^2\right\}dr - 8\sum_{n=1}^{\infty} e^{-\gamma_n^2 t/\tau} \frac{1}{\gamma_n^3 J_1(\gamma_n)} \int_o^{r_o} r\, J_o\left(\gamma_n \frac{r}{r_o}\right)dr\right].$$

The second integral is evaluated by use of the recurrence relation

$$\frac{d}{dz}\left(z\, J_1(z)\right) = z\, J_o(z)$$

which, by integrating both sides gives

$$z\, J_1(z) = \int z\, J_o(z)\, dz$$

or, putting

$$z = \gamma_n \frac{r}{r_o}$$

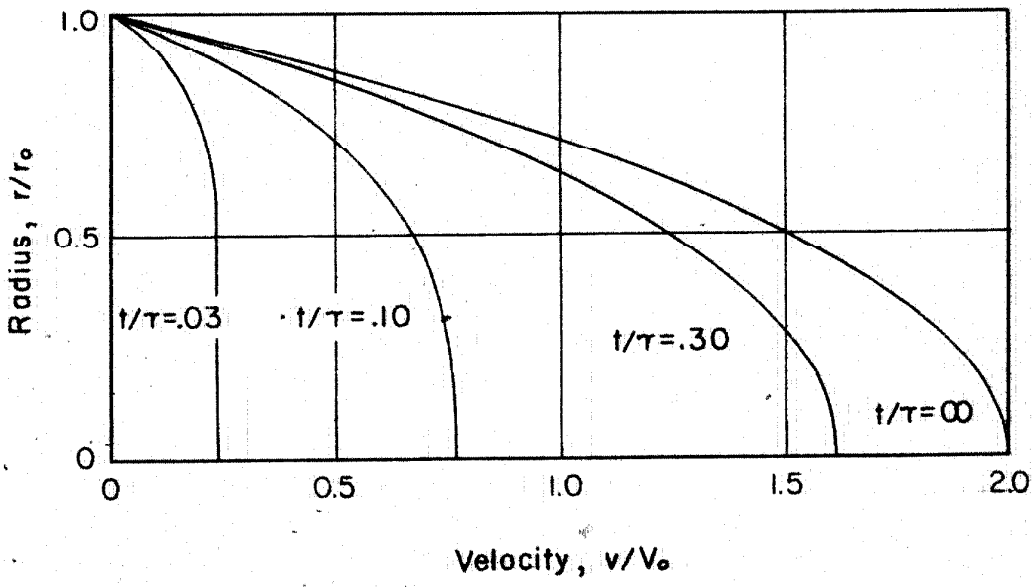

Fig.9 Velocity Profiles, r/r_o vs. v/V_o, at Several Times, t/τ

gives

$$\int \gamma_n\left(\frac{r}{r_o}\right) J_o\left(\gamma_n \frac{r}{r_o}\right) d\left(\gamma_n \frac{r}{r_o}\right) = \gamma_n\left(\frac{r}{r_o}\right) J_1\left(\gamma_n \frac{r}{r_o}\right)$$

or

$$\int r\, J_o\left(\gamma_n \frac{r}{r_o}\right) dr = \frac{r_o}{\gamma_n} r\, J_1\left(\gamma_n \frac{r}{r_o}\right).$$

Substituting the limits

$$\int_o^{r_o} r\, J_o\left(\gamma_n \frac{r}{r_o}\right) dr = \frac{r_o^2}{\gamma_n} J_1(\gamma_n),$$

then V becomes

$$V = \frac{4V_o}{r_o^2}\left[\frac{r_o^2}{4} - 8\sum_{n=1}^{\infty} e^{-\gamma_n^2 \frac{t}{\tau}} \frac{r_o^2}{\gamma_n^4}\right]$$

or

$$\frac{V}{V_o} = 1 - 32 \sum_{n=1}^{\infty} \frac{e^{-\gamma_n^2 \frac{t}{\tau}}}{\gamma_n^4} . \qquad (19)$$

This series converges even more rapidly than the one in equation (18). Values of $\frac{V}{V_o}$ vs the time parameter $\frac{t}{\tau}$ are plotted in Fig. 10.

From these results it may be seen that a close approximation to steady flow conditions may be obtained within any desired time interval by proper choice of the characteristic time constant τ. In the design of this machine the criterion was used that steady flow conditions are approximated sufficiently closely in a time 0.3τ, and that this time should be relatively small compared to the rise time, T, of load in the machine.

The numerical values of the various design constants of the machine as used in the present investigation are:

area of the loading piston, $A_1 = 49.4$ in.^{2},

area of the actuating piston, $A_2 = 4.90$ in.^{2},

sum of the cross-sectional areas of the damping tubes, $A = 4.45$ in.^{2},

length of the damping tubes, $L = 6$ in.,

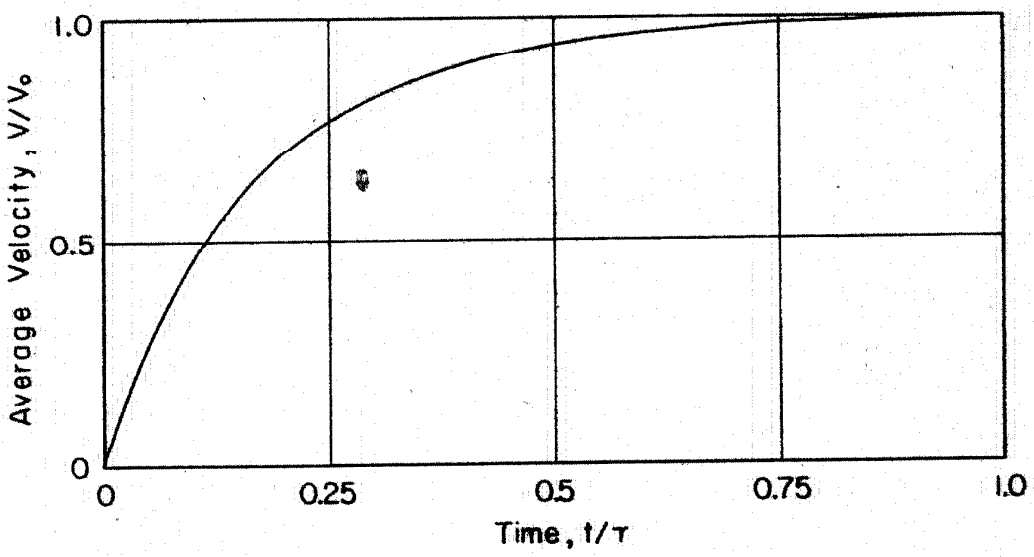

Fig.10 Average Velocity, V/V_o, vs. Time, t/τ

inside radius of the damping tubes, r_o = 0.0395 in.,

viscosity of damping fluid

μ = 300 centipoise = 4.4×10^{-5} lb sec/in.^{2},

specific gravity of damping fluid = 0.045 lb/in.^{3},

obtained with a glycerine-water solution of 93 per cent glycerine.

From the detailed dimensions of the machine the equivalent mass and the spring constant are computed to be:

$$M \times g = 540 \text{ lb},$$

$$K = 350{,}000 \text{ lb/in.},$$

where g is the acceleration due to gravity.

Using these values the various parameters which characterize the operation of the machine are computed to be:

critical damping coefficient, equation (1),

$$C_{cr} = 1400 \text{ lb sec/in.},$$

damping coefficient computed for viscosity used, equation (10),

$$C = 730 \text{ lb sec/in.} = 0.52\, C_{cr},$$

time constant for damping tube flow, equation (17),

$$\tau = 4.2 \times 10^{-3} \text{ sec},$$

conventional load rise time, equations (3) and (4),

$$T = 5.4 \times 10^{-3} \text{ sec}.$$

The actual viscosity used, leading to a theoretical damping coefficient of 0.52 times the critical damping coefficient, was determined by trial and error to find the best experimental load vs. time relation for "free loading" of a specimen within its elastic range. Two experimental

load-time curves of this type are shown in Fig. 11 where they are compared with the computed curves for critical damping and 0.52 critical damping. The straight line corresponding to the conventional load rise time, T, is also shown in the figure. The variations of the experimental curves from the computed curve for 0.52 critical damping are probably due primarily to the damping contributed by the friction of the "O" ring piston seals.

B. Specimen Heat Exchanger

The specimen heat exchanger, shown in Fig. 3, consists of two essentially identical heads into which the ends of the specimen are threaded. A metal bellows which surrounds the specimen is attached to the two heads by threaded rings. Each head contains a temperature control fluid header and a water jacket. The fluid headers are connected with the annular space between the specimen and metal bellows by several circumferentially spaced holes. The temperature control fluid is pumped into one of the fluid headers through a fitting (not shown in Fig. 3) in the side of the header. It is discharged through a similar fitting in the other header. In this way a continuous flow of the temperature control fluid may be maintained around the specimen throughout a test. The metal bellows extends as the specimen extends. The total extension is limited to 0.05 in. by the limited travel of the actuating piston of the testing machine as mentioned previously. The force required to extend the bellows is insignificant compared to the load acting on the specimen. The water jackets serve to prevent heating or cooling of the adjacent portions of the

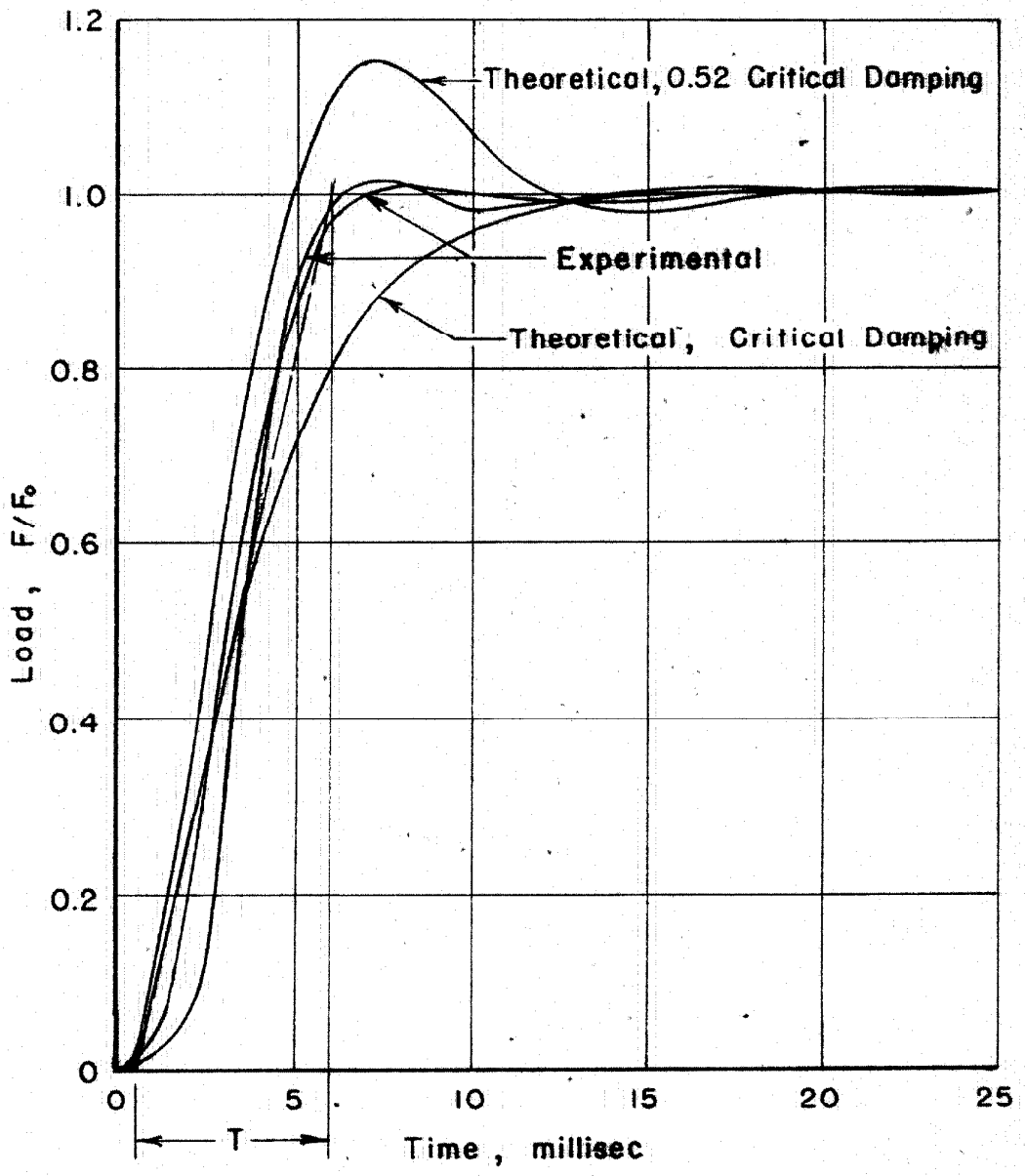

Fig.11 Theoretical and Experimental Load vs. Time for Free Loading with Elastic Specimen

testing machine. Fresh water is continuously circulated through these jackets during a test. The water connection fittings are not shown in Fig. 3.

The heat exchanger is fitted with suitable stuffing boxes through which thermocouples may be inserted to measure the specimen temperature. A "V" groove is provided on the outside of each of the temperature control fluid headers which serve as gage points for the extensometer. The extreme ends of the heat exchanger are threaded to fit the dynamometer and the lower or moving head of the testing machine.

C. Dynamometer

Detection of the load acting on the specimen during a test is accomplished by means of the dynamometer of the resistance sensitive type shown in Fig. 3. Four Baldwin Southwark Type AB-14 bakelite bonded gages are cemented to the hollow cylindrical reduced section of the dynamometer body, with their filaments parallel to the axis of the dynamometer. The four gages are connected in series, giving a total resistance of approximately 2000 ohms. The body of the dynamometer consists of SAE x4130 steel, heat treated to a hardness of 35 R_c. The reduced section is designed for a stress of approximately 100,000 lb/in.^{2} at the maximum machine load of 10,000 lb. A brass sleeve provides mechanical protection and electrostatic shielding for the winding.

A calibration of the dynamometer has been made in which its resistance change was measured as a function of load. Resistance changes were measured with a Wheatstone bridge having a sensitivity of 0.01 ohm, and the load was applied and

measured by a Riehle Universal testing machine having a least reading of 10 lb. The calibration curve obtained is given in Fig. 12. The calibration constant is 784 lb/ohm. The natural frequency of this dynamometer has not been measured. However, previous experience with dynamometers of similar construction and size has indicated that the natural frequency is about 50,000 cycle/sec, which is much higher than required for use with the rapid load testing machine.

Temperature compensation of the dynamometer is provided by a 2000 ohm dummy dynamometer of essentially identical mechanical and electrical construction, which is used as the second leg of the voltage dividing circuit in which the dynamometer is connected.

D. Extensometer

The extensometer, shown in Fig. 3, consists of two essentially identical elements placed on opposite sides of the specimen heat exchanger and clamped together against the heat exchanger. The heat exchanger is provided with two "V" grooves which locate the four knife edges of the extensometer. When the specimen is strained, the resultant relative motion of the knife edges causes a small beam in each element of the extensometer to bend. Two Baldwin Southwark Type AB-14 bakelite bonded SR-4 resistance sensitive wire strain gages of 500 ohms resistance each are mounted on each side of each beam with their filaments lying in the direction of the bending stresses. Thus there is a total of eight 500 ohm gages. They are electrically connected in series in two sets of four, giving 2000 ohms in each set, and the gages of the two sets are subjected

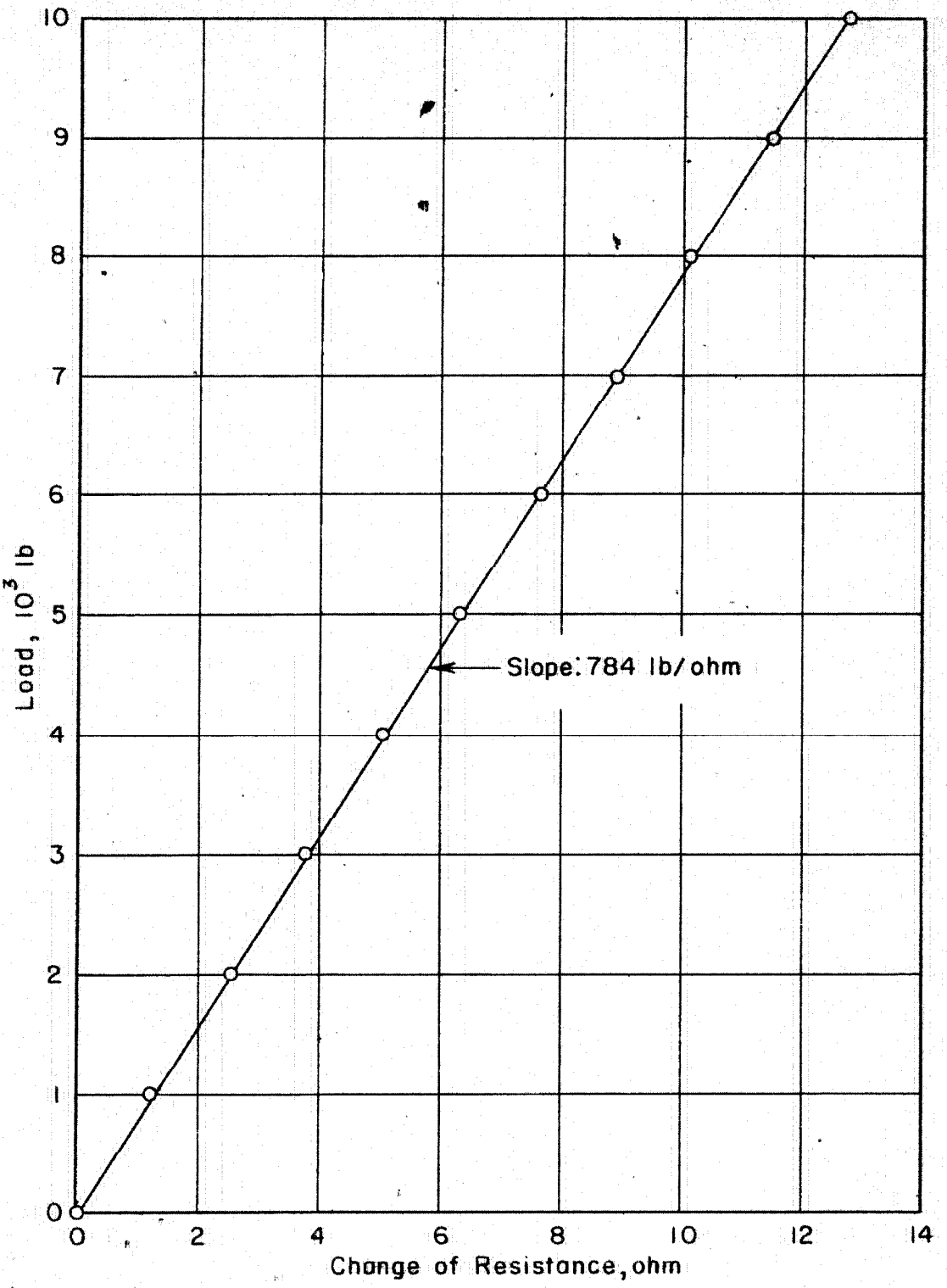

Fig.12 Dynamometer Calibration Curve

to stresses of opposite sign. The two sets are used as the two legs of a voltage divider, thus providing temperature compensation of the gages without the use of an inactive dummy gage.

This extensometer provides a permanent extension measuring unit and avoids the difficulties encountered by cementing resistance sensitive gages directly on the specimen. However, it introduces one error in the extension measurements which consists of the strains which occur in the shoulders of the test specimen and in the heads of the heat exchanger. The effects of this error and its correction are discussed later. The beams of the extensometer are designed to have a fundamental natural frequency of about 2800 cycle/sec, which is sufficiently high to prevent excitation of the normal modes of vibration during the extension of the specimen.

The extensometer was calibrated by means of the calibrator, shown in Fig. 13, and a Wheatstone bridge. The smallest divisions of the dial gage used in the calibrator are 0.0001 in. and readings were estimated to 0.00005 in. The dial gage was checked against Dearborn gage blocks and was found to have a maximum error of 0.00025 in. over its total range of 0.050 in. The sensitivity of the resistance measurements was 0.01 ohm. The change in resistance measured was equal to the sum of the absolute values of the changes in resistance of the two active legs of the extensometer. The calibration curve obtained is shown in Fig. 14. The calibration constant, given by the slope of the line, is equal to 5.73×10^{-3} in./ohm.

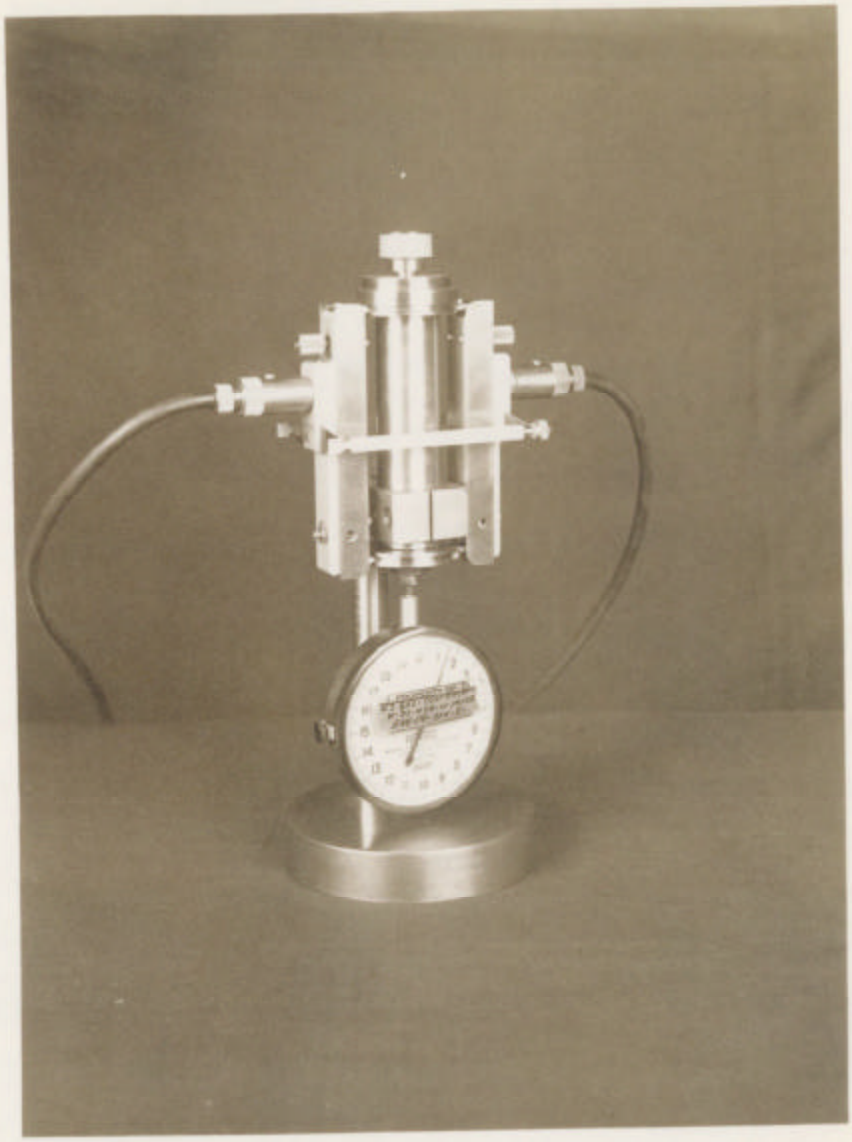

Fig.13 Calibrator with Extensometer in Position

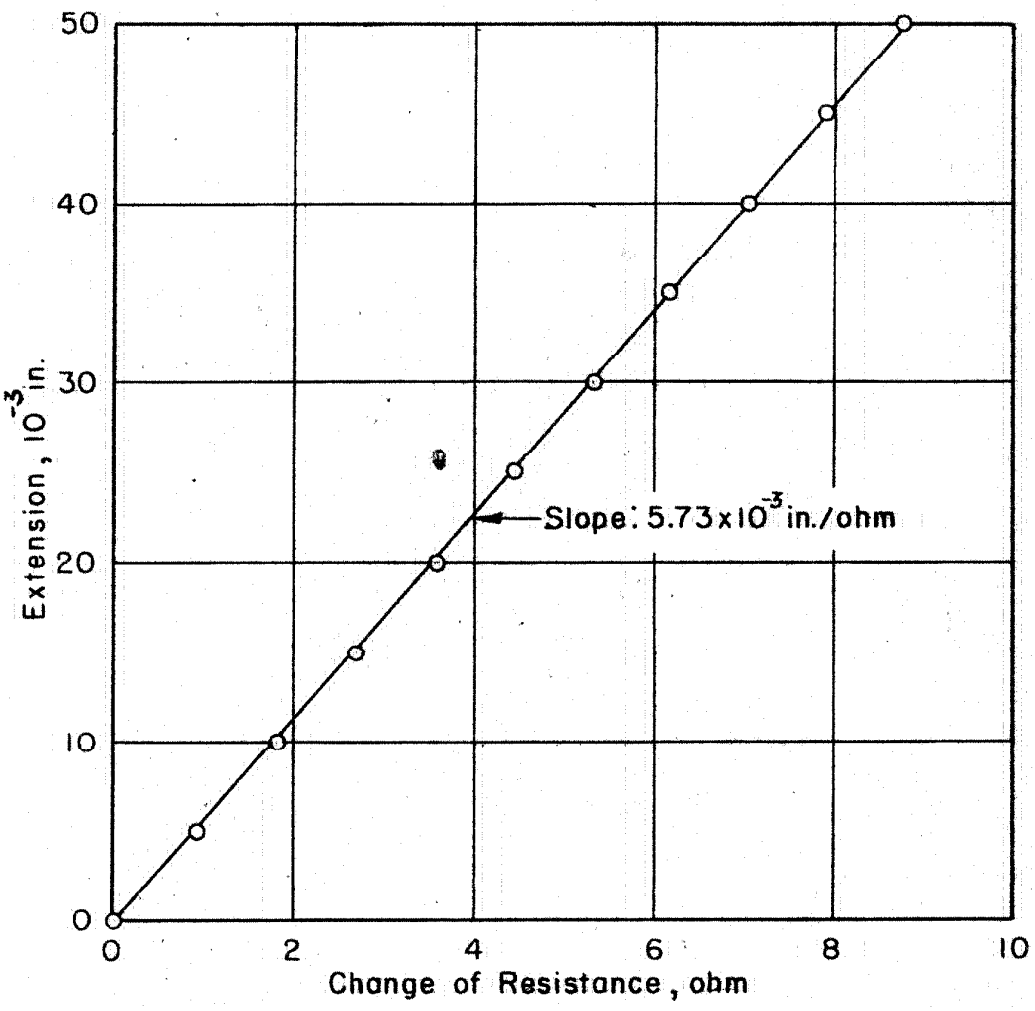

Fig. 14 Extensometer Calibration Curve

E. Recording Unit

The recording unit consists of two identical channels, one for measurement of load on the specimen and the other for extension measurement. The principal element in each channel is an RCA Type 327A Cathode Ray Oscilloscope. A schematic block diagram of one of the two channels is shown in Fig. 15, and a photograph of the recording unit is presented in Fig. 4. The dynamometer and extensometer are connected in simple 1:1 voltage dividing circuits. For the former instrument one leg of the voltage divider consists of a dummy dynamometer of equal resistance and of similar mechanical construction to provide a voltage divider having symmetrical characteristics with respect to temperature, drift, capacity, and inductance. In the case of the extensometer both legs of the circuit are incorporated in the instrument and both are active. Calibration of the signal is provided by a known high resistance shunt which is connected by a relay across one leg of the voltage divider at the proper time during a single sweep of the oscilloscope. The time of closing of the calibration relay is automatically synchronized with the beginning of the calibration sweep by suitable relay delay circuits so that a vertical step is formed on the oscilloscope screen near the center of the calibration trace. The resistance of the calibration resistor, the two legs of the voltage divider, and the calibration constant of the instrument are known; therefore, the height of the vertical step on the calibration trace may be converted to a known number of units of the quantity being measured. The sensitivity of the recording system can be

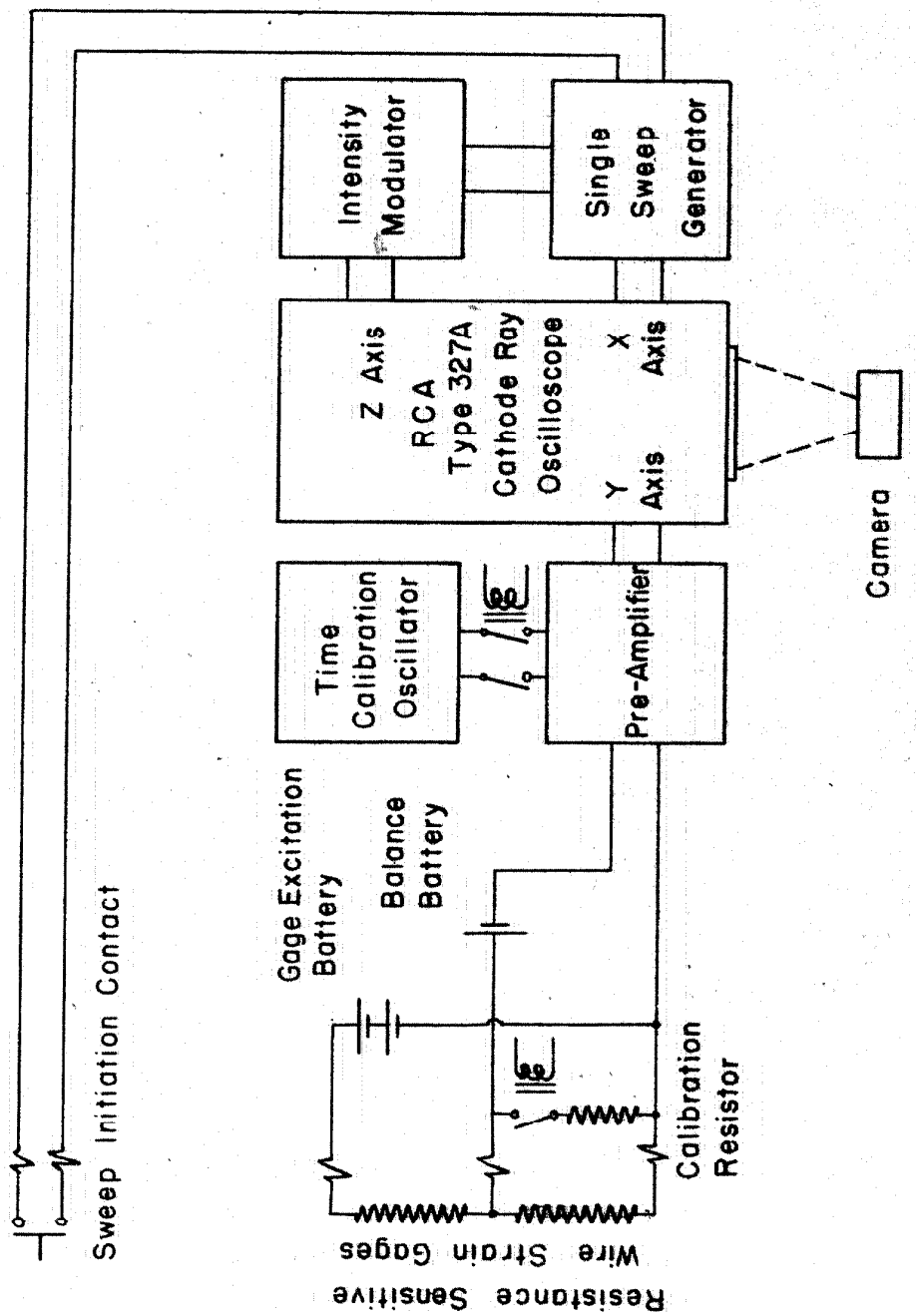

Fig.15 Schematic Block Diagram of One Channel of Recording Unit

adjusted by changing the voltage supplied to the circuit by the gage voltage battery. The maximum voltage used is 1½ volts.

In order to maintain sensitivity of the recording system for time intervals of several seconds, which are required in the rapid load tests, a direct coupled pre-amplifier is used together with the direct coupled amplifier incorporated in the oscilloscope. This necessitates a balancing battery in the pre-amplifier input line to block the D.C. voltage on the resistance sensitive gage from the pre-amplifier grid and provide proper pre-amplifier grid bias. The pre-amplifier consists of a single-stage two-tube balanced amplifier having a fixed voltage gain of approximately 10. The maximum sensitivity of the oscilloscope is approximately 70 mv/in., making the maximum sensitivity of the complete amplification system approximately 7 mv/in. oscilloscope deflection. This sensitivity is more than adequate, and the amplifiers are normally operated at reduced gain settings.

Time calibration of the sweep is provided by the time calibration oscillator which applies sharp vertical markers on a separate trace on the oscilloscope screen. The timing oscillator consists of a Hewlett-Packard Model 200C variable frequency oscillator and a circuit to convert the sine wave output of the variable frequency oscillator into sharp peaked time markers at the same frequency. For precise frequency setting, the timing oscillator frequency is compared with a crystal controlled frequency from a Hewlett-Packard Model 100A secondary frequency standard by means of a small auxiliary

oscilloscope.

Sweep times from 0.1 millisec to 10 sec are supplied by the sweep generator. During a test the sweep is initiated by the switch shown on the diagram, which is located in the actuating unit of the testing machine. This switch is closed when the cam reaches a certain position in its travel. The position of the switch may be adjusted so that the sweep is initiated a short time before loading of the specimen begins. The basic circuit of the sweep generator consists of a condenser and a constant current tube. The condenser discharges through the tube when the tube is triggered by the closing of the sweep initiating switch in the testing machine. The resulting linear voltage drop of the condenser is applied to the X axis of the oscilloscope, giving a linear sweep. The sweep may also be initiated by other manual and automatic switches in order to produce the vertical and timing calibration traces.

The intensity modulating unit is used to blank out the cathode ray tube at all times except during sweeps. The triggering impulse required to turn on the oscilloscope beam is supplied by the sweep generarator.

The oscilloscope screen is photographed on 35 mm recording orthochromatic film, by means of a Zeiss Biotar f:1.4 lens or a Zeiss Sonnar f:1.5 lens. The records consist of three traces, a horizontal timing trace, a vertical calibration stepped trace, and the signal from the dynamometer or extensometer. A robot control is incorporated in the recording unit which operates the room lights and the camera shutters,

applies the timing and vertical calibration traces, and triggers the testing machine.

The controls for the drive unit and a tachometer indicating the speed of the rotor of the testing machine are also mounted on the recording unit panel.

F. Alcohol Cooling and Circulating Unit

For the tests made at temperatures below room temperature, denatured ethyl alcohol cooled by solid carbon dioxide is used as the temperature control fluid. The cooling bath and a circulating pump are contained in an insulated box which may be seen in Fig. 5. The alcohol which is circulated through the specimen heat exchanger is isolated from the alcohol-solid CO_2 coolant bath. The circulated alcohol is contained in a small tank and a coil of tubing which is suspended in the coolant bath together with the circulating pump. This arrangement is necessary because the alcohol of the coolant bath cannot be pumped readily due to the CO_2 vapor which it contains. This vapor prevents proper operation of the pump. This unit was designed and constructed by Mr. David A. Elmer and is described in his thesis (23).

G. Oil Heating and Circulating Unit

For tests made at temperatures above room temperature, mineral oil heated by an electric immersion heater is used as the temperature control fluid. The tank in which the oil is heated, and the circulating pump and necessary valves and controls are assembled together to form the oil heating and circulating unit. This unit is shown in the photograph in Fig. 6. The heater tank has a capacity of 15 gal and is vented to the

atmosphere. It contains a 4 kw electric immersion heater and the temperature sensitive element of a Partlow Model ZO-6K automatic temperature controller. The circulating pump is an electric motor driven gear pump having a capacity of 8 gal/min. A pressure relief valve is provided in a by-pass line between the pump discharge and the return line to the tank to prevent excessive pressures in the system, and to provide for internal circulation of oil in the unit when the fluid circuit to the specimen heat exchanger is closed off.

The unit is operated on 220 volt single phase A.C. power, and is mounted on casters. Suitable insulated pipes and flexible metal hoses are provided in the laboratory for connecting the unit to the specimen heat exchanger. The electric power connections to the pump drive motor and the heating element are such that the pump is always running when the unit is in operation. This insures a continuous circulation of oil over the heating element under all circumstances of operation. Thus the fire hazard is reduced by minimizing the possibility for local heating of the oil, near the heating element, to excessive temperatures.

For temperatures above about 250°F Martemp quenching oil, supplied by E. F. Houghton Co., having flash and fire points of 530°F and 590°F respectively, is used in the unit. For temperatures below about 250°F SAE 10 lubricating oil is used. The lower viscosity of the latter oil at the lower temperatures reduces the tendency for cavitation in the pump suction passages.

It has been found experimentally that when the unit is

connected to the specimen heat exchanger in the manner used in this investigation, the temperature of the test specimen may be maintained continuously at a maximum temperature of approximately 400°F. It has also been found that the temperature of the test specimen varies over a total range of 7°F for a fixed setting of the temperature controller.

H. Static Test Equipment

Static tension tests were made using a 30,000 lb Riehle testing machine having a least reading of 10 lb. For tests at room temperature the strain in the specimen was measured in three different ways. A pair of Huggenberger extensometers, with their gage points on the gage section of the specimen, were used to measure accurately the strains within the elastic limit. These gages have a total range of approximately 6×10^{-3} in./in. or 0.6 per cent with 40 divisions of 1.5×10^{-4} in./in. each. Readings were estimated to 1/5 division or 3×10^{-5} in./in.

Strains up to a total of 5 per cent were measured by means of two Federal Model E3B dial gages having a total range of 0.050 in. and divisions of 10^{-4} in. Readings were estimated to 0.5×10^{-4} in. The two dial gages on opposite sides of the specimen were fastened to the upper static test specimen grip, and their spindles were actuated by adjustable rods fastened to the lower grip.

Strains from 5 per cent to failure were measured by means of two steel scales, one on each side of the specimen. The scales were graduated in 1/32 in. divisions and readings were made to 1/10 of a scale division by means of a vernier.

Because the dial gages were attached to the specimen grips their indications of strains were too large by the strains in the shoulders of the test specimen and in the grips. By comparing the apparent modulus of elasticity given by the dial gage measurements with the correct modulus obtained from the Huggenberger strain gage measurements, the strains computed from the dial gage measurements were corrected for the elastic strains in the grips and in the shoulders of the specimen.

For static tension tests at temperatures other than room temperature, the specimen was mounted in the same specimen heat exchanger used for the rapid load tests. The same cooling and heating units used for the rapid load tests were also used to control the specimen temperature in the static tests. Extension of the specimen was measured by means of the extensometer used in the rapid load tests in conjunction with a Wheatstone bridge. By comparing the apparent modulus of elasticity indicated by the extensometer with the known modulus of elasticity of the material, a correction was made for the elastic strains in the heads of the specimen heat exchanger and shoulders of the specimen. The maximum extension of the specimen in static tests made at temperatures other than room temperatures was limited to 5 per cent strain by the permissible extension of the metal bellows of the heat exchanger.

I. Temperature Measurement Equipment

The temperature of the test specimen was measured by means of copper-constantan thermocouples and a Leeds and

Northrup portable precision potentiometer for all tests except those made at room temperature. In the latter case temperatures were read from a mercury thermometer hung near the testing machine. For tests at temperatures other than room temperature a maximum of four and a minimum of two thermocouples were used in each test. In every test one thermocouple was placed near the center of the gage section of the specimen and one on one of the specimen fillets. Both of these couples were covered by tape wrapped around the specimen and the couples. In some tests two additional thermocouples, inserted into holes drilled in the ends of the specimen, were used. The positions of the thermocouples are indicated in Fig. 3. The difference in the temperatures measured at the center of the specimen gage section and at the fillets was found to be not more than $1^{\circ}F$ in all cases, while the temperatures measured in the holes in the ends of the specimen were 2 to $3^{\circ}F$ nearer room temperature than the temperature at the center of the gage section. All of the thermocouples used were made of thermocouple wire taken from the same spools of copper and constantan wire. One thermocouple made of wire from these spools was calibrated at four fixed temperature points. A satisfactory agreement with the Bureau of Standards 1938 calibration for copper-constantan thermocouples was found. This calibration and its results are discussed later in this thesis.

While rapid load tests were being performed a thermocouple in the end or on the shoulder of the specimen was connected to a Leeds and Northrup "Micromax" temperature recorder.

This provided a convenient visual indication which aided in the adjustment of the temperature to the desired value.

III. METHOD OF ANALYSIS OF THE RAPID LOAD TEST RECORDS

The photographic records were enlarged approximately eight times by projecting them and tracing the record lines carefully by hand. The height of the records on these tracings was from 2 to 4 in., and the total length of the horizontal time axis of the records was about 4 in. Tracings of a typical record and the measurements made on the traces are shown in Fig. 16. All measurements of distances on the traces were made with a scale having 1/50 in. divisions, and the numbers representing distances in the figure are in units of 1/50th in.

The record tracings shown in Fig. 16 represent the test for which the primary data are as follows.

Specimen No.	63.
Diameter of gage section . . .	0.2999 in.
E.M.F. of copper-constantan thermocouple at center of specimen gage section with respect to a cold junction at 32°F	-2.111 millivolts.
Frequency of both time calibration traces.	50 cycle/sec.
Dynamometer calibration constant	784 lb/ohm.
Load record calibration resistance change.	6.74 ohm.

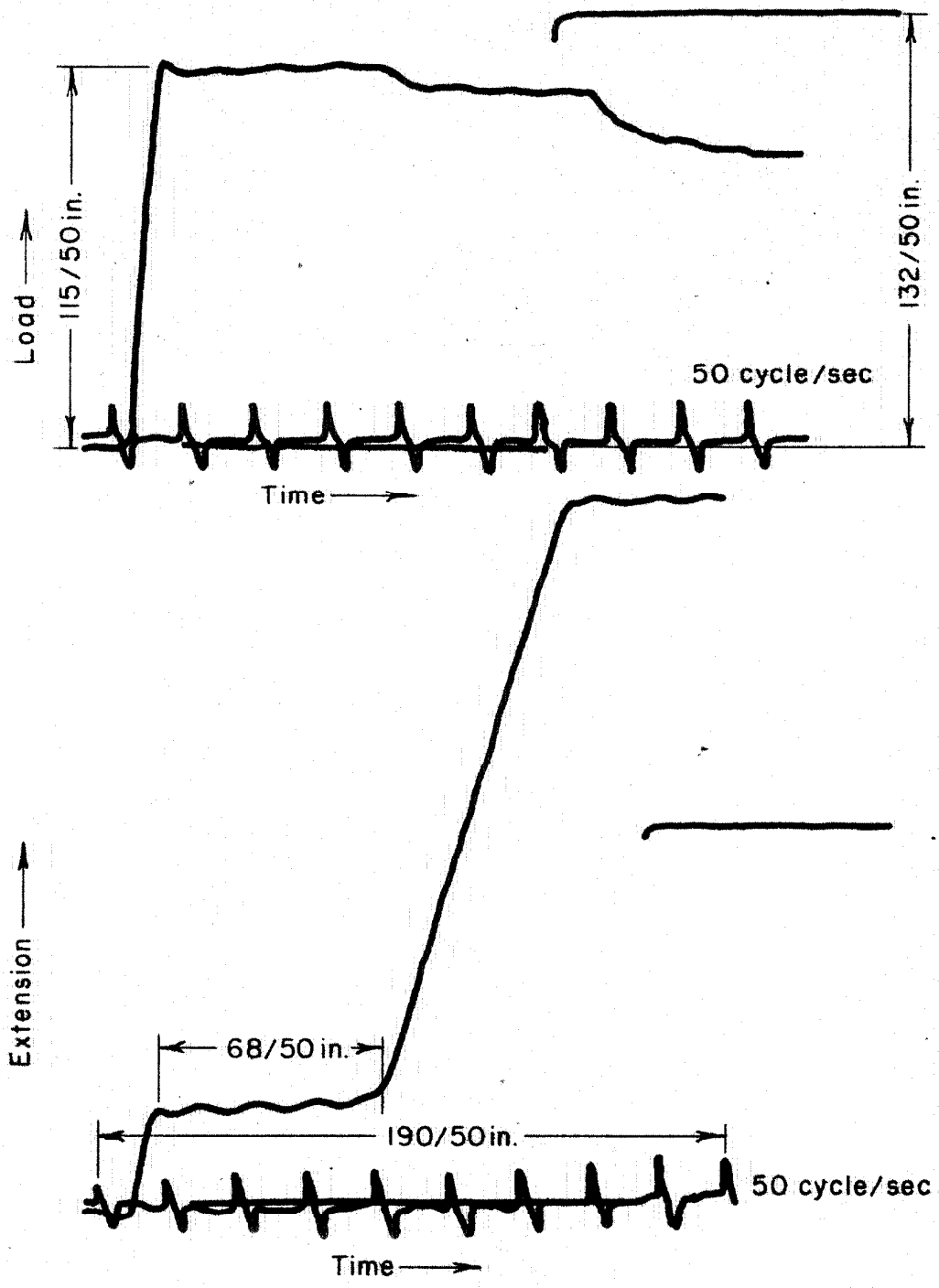

Fig.16 Tracing of a Typical Record,
Specimen No.63 Tested at −74.5 °F

Extensometer calibration

constant . . . . . 5.73×10^{-3} in./ohm.

Extension record calibration

resistance change. . . . . 3.37 ohm.

The measurements made on the records are as follows.

Height of load record calibration

trace. . . . . 132/50 in.

Height of load trace during

period of elastic deformation. . 115/50 in.

Number of timing wave cycles

included in time calibration

distance measured on extension

record . . . . . 9.

Time calibration distance

measured on extension record . . 190/50 in.

Measured distance corresponding

to the time to initiate elastic

deformation. . . . . 68/50 in.

The computation of the measured stress for the test is as follows.

Cross sectional area of test specimen,

$$A = \frac{\pi}{4}(0.2999)^2 = 0.0707 \text{ in.}^2$$

Stress corresponding to the height of the

load record calibration trace,

$$= \frac{784 \times 6.74}{0.0707} = 74{,}800 \text{ lb/in.}^2$$

Stress during the period of elastic deformation,

$$= 74{,}800 \times \frac{115}{132} = 65{,}200 \text{ lb/in.}^2$$

The computation of the measured time to initiate plastic deformation from the extension record is as follows.

Total time included in time calibration for distance measured,

$$= 9 \times \frac{1000}{50} = 180 \text{ millisec.}$$

Time to initiate plastic deformation,

$$= 180 \times \frac{68}{190} = 64 \text{ millisec.}$$

Although no measurements of the magnitudes of the extensions were made for the present investigation, the vertical step calibration traces were included on all records in order to permit the determination of extensions from the records in the future, if such measurements should become of some interest. Similarly the time calibration trace was included on all load records.

IV. ACCURACY OF MEASUREMENTS

In estimating the degree of accuracy of the measurements reported, two general types of experimental error are distinguished. The first may be called absolute error. An example is the difference between loads read on the static testing machine and loads which would be given by standard weights. The second type consists of the errors introduced by the lack of reproducibility of the various measurements, which may be called random errors.

The static tension tests and the dynamometer calibrations were all performed on the same testing machine. Also the resistance changes corresponding to the oscilloscope calibration traces were measured with the same Wheatstone bridge used in the calibrations of the dynamometer and extensometer. Therefore stresses and strains measured in the rapid load tests are subject to the same absolute error as those measured in static tests.

Absolute errors in the stress measurements may arise from three sources, the error of the 30,000 lb Riehle testing machine, the error in measurement of the diameter of the gage section of the specimen, and the stress concentration associated with the specimen fillets. The testing machine is calibrated yearly and its error is found to be not more ± 1 per cent. Specimen diameters were measured with a good micrometer caliper, estimating to 0.0001 in., so that the error from this source is negligible. The stress concentration in the specimen fillets introduces a constant bias error in all determinations

of the upper yield stress. This includes static upper yield stress determinations and all the stress measurements reported for the rapid load tests, since the latter are all measurements of upper yield stress. This error may be estimated from stress concentration factors determined photoelastically by Frocht (24), for fillets in flat bars. Frocht's measurements do not include ratios of fillet radius to width of the reduced section of the bar as large as that of the specimen used in the present investigation. However, an extrapolation of his data leads to a stress concentration factor of about 1.03. Other photoelastic measurements have shown that the stress concentration factor for a round bar of a given ratio of fillet radius to diameter is only slightly less than for a flat bar having the same ratio of fillet radius to the width of the bar. Hence, it is reasonable to assume that the bias in measurements of upper yield stress due to stress concentration is not more than 3 per cent, the measured stresses always being too low.

Since this investigation was concerned only with the time to initiate plastic deformation, quantitative measurements of strain during the rapid load tests were not made. Therefore, errors in strain measurement in the rapid load tests need not be considered. However, the probable absolute errors in strain measurements in the static tests may be of some interest. For the static tests made at room temperature such errors could be contributed by the error of the two Huggenberger extensometers, and the error due to neglecting plastic strain in the fillets of the test specimen. The first

is estimated to be not more than ± 2 per cent, while the latter may be as large as 10 per cent. For static tests made at temperatures other than room temperature absolute errors could arise from the error of the dial gage used in the extensometer calibration, and from the plastic strain in the fillets of the test specimen. As mentioned previously, the dial gage was checked against gage blocks and found to have a maximum error of 0.00025 in. in its total range of 0.050 in., or 0.5 per cent. The plastic strain in the specimen fillets is 10 per cent or less as given above.

The absolute error in the time measurements in the rapid load tests is estimated to be ±0.2 per cent, which represents the probable error of the quartz crystal oscillator used as a time standard.

The random errors of the measurements were estimated from the results of experiments made for that purpose. To estimate the random errors in the calibration constants of the dynamometer and extensometer, a statistical study of the calibration data was made. A calibration constant was computed for every pair of measurements of load (or extension) and resistance change made in one dynamometer and in one extensometer calibration. For the dynamometer, 22 values of the calibration constant had a standard deviation about the mean of 0.9 per cent. For the extensometer, 18 values had a standard deviation about the mean of 0.8 per cent.

A major portion of the random errors may be attributed to recording and record reading errors. Recording errors were

caused by non-linearity, pick-up of stray fields, and instability of the pre-amplifiers and oscilloscope amplifiers, and interaction between the various amplifiers. Reading errors are introduced in the process of tracing the enlargements of the photographic records and in the measurement of distances on the tracings.

It is difficult to estimate the random errors from these sources separately; however, one experiment was made which gives some indication of the over-all error. This experiment consisted of performing a calibration of the extensometer using the recording system to measure resistance changes, in place of the Wheatstone bridge. Such an experiment is made possible by the direct coupled amplifying system. The extensometer was mounted on the calibrator and connected to the recording system as for a rapid load test. The calibrator was set for zero extension of the extensometer and a single trace was produced on the oscilloscope and recorded. Then a given extension was applied to the extensometer and a second oscilloscope trace recorded. Finally, a record calibration trace was recorded, all three traces being recorded on one film within a few seconds. This procedure was repeated for several different values of the extension applied to the extensometer.

Analysis of the records so obtained was made in the usual manner, and values of the extensometer calibration constant were computed from the results. These values had a standard deviation about the mean of about 3 per cent, and the difference between the calibration constant determined in

this manner and the constant found in the calibration using the Wheatstone bridge was also about 3 per cent. From this result it appears reasonable to assume that the random errors in the stress measurements in the rapid load tests, due to the recording and reading errors, were about ± 3 per cent.

An estimate of the random error in the time measurement, due to recording and reading errors, was obtained by analyzing in detail the timing traces of two rapid load test records. A relation between linear distance on the record tracings and time was determined in the usual manner. Then by measuring the distances from a timing wave peak near one end of a record to each individual wave peak in the timing trace, deviations from the linear time scale were determined. A total of 73 such measurements was made and the standard deviation of these measurements from the linear relation was 0.6 per cent of the total length of the time trace. An additional random error in time measurement of about ± 0.2 per cent or less was introduced in the operation of comparing the frequencies of the standard and working oscillators.

Since the random error in the measurement of the delay time is proportional to the total length of the time trace, the percentage error in the measurement of the delay time depends upon the ratio of the delay time to the length of the time trace. It is not possible to perform the tests so that the delay time is always a major proportion of the time trace. It may be from one tenth to nine tenths of the delay time. Therefore the random error is different for each test. The values of the delay time reported for this investigation are

stated to the appropriate number of significant figures.

All thermocouples used in the temperature measurements were taken from the same spools of copper and constantan thermocouple wire. The reference junction was immersed in a water-ice bath for all measurements. The thermocouple wire used was calibrated at four fixed temperature points as follows:

freezing chloroform . . . . . -82.3°F,
freezing mercury. . . . . -38.0°F,
freezing carbon tetrachloride . . . . -9.2°F,
and body temperature. . . . . 98.6°F.

The temperatures determined at these points, using the Bureau of Standards 1938 calibration for the relation between e.m.f. and temperature, were within ± 1°F of the above standard values in all cases.

In performing the rapid load tests the specimen temperature was determined immediately before running the test, and in many cases the temperature was also determined immediately upon completion of the test. It was found that the temperature change during the period required to run the test was 1°F or less. From these results it is reasonable to assume that the accuracy of determining the temperature of the test specimen was ± 2°F.

To summarize, the estimated magnitudes of the various errors are as follows.

(1) Absolute error in all stress measurements contributed by the static testing machine, ≤ ± 1 per cent.

(2) Constant bias in all measurements of upper yield stress due to stress concentration in the fillets of the test specimen (measured stress always less than true value), ≤ 3 per cent.

(3) Absolute error in static elastic strain measurements, $\leq \pm 2$ per cent.

(4) Bias in measurements of static plastic strains (measured strain always greater than true value), ≤ 10 per cent.

(5) Absolute error in time measurements, $\leq \pm 0.2$ per cent.

(6) Random error in stress measurement in rapid load tests, $\leq \pm 4$ per cent.

(7) Random error in measurement of delay time, variable.

(8) Random error in temperature measurement, $\leq \pm 2^{\circ}F$.

V. MATERIAL TESTED AND TEST SPECIMEN

The 0.17 per cent carbon steel used in this investigation was obtained from the Columbia Steel Company, Torrance, California Works. It was hot rolled to 5/8 in. diameter bars from one billet of heat number 32862. The analysis as given by the mill is as follows:

Carbon	0.17%,
Manganese	0.39%,
Phosphorous	0.017%,
Sulphur	0.040%.

Test specimens, of the form shown in Fig. 17, were machined from this material. The gage section of the specimens was finished by grinding. After machining, the specimens were annealed in dry hydrogen. The furnace schedule was as follows:

1. heat from room temperature to 1300°F at normal furnace rate under full power,
2. heat from 1300°F to 1600°F at 2.4°F per min,
3. hold at 1600°F for 49 min,
4. cool from 1600°F to 1300°F at 2.3°F per min,
5. cool from 1300°F to 1000°F at 3.2°F per min,
6. cool from 1000°F to room temperature at normal furnace rate with power off.

The resulting metallographic structure is shown in two photomicrographs in Fig. 18. One of the photomicrographs was taken of a transverse section of the test specimen and the

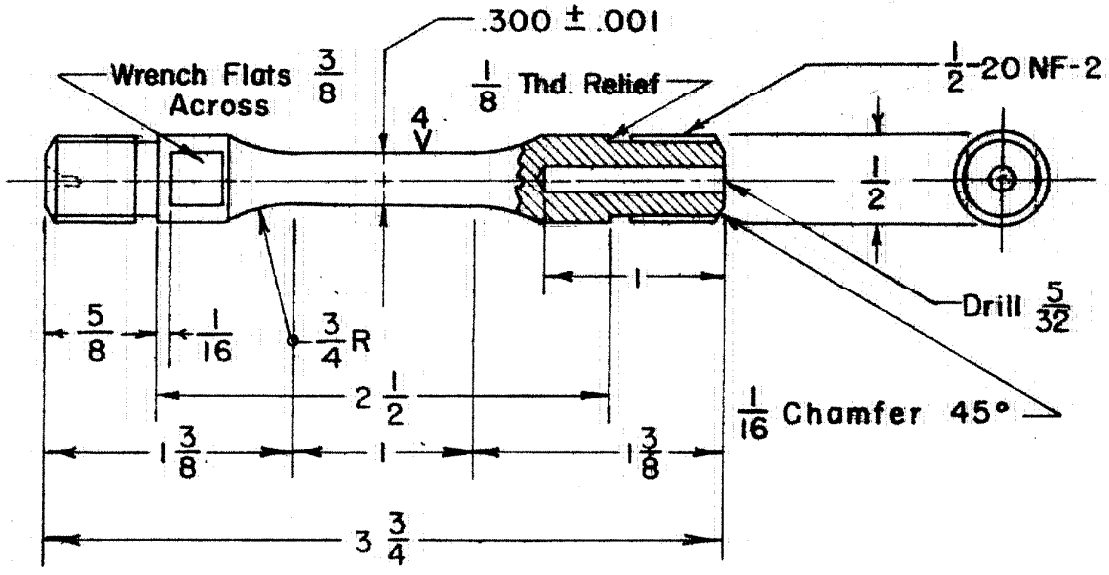

Fig.17 Test Specimen

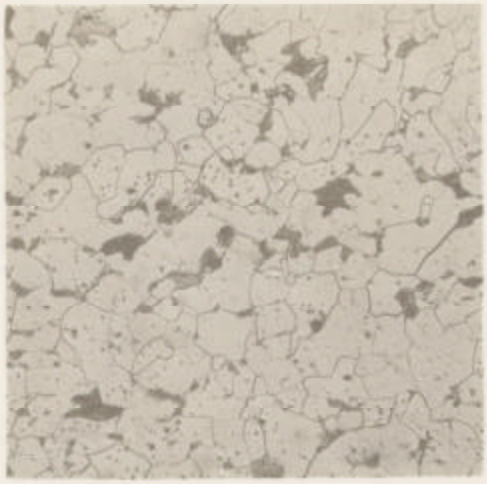

Nital Etch X200

Transverse Section

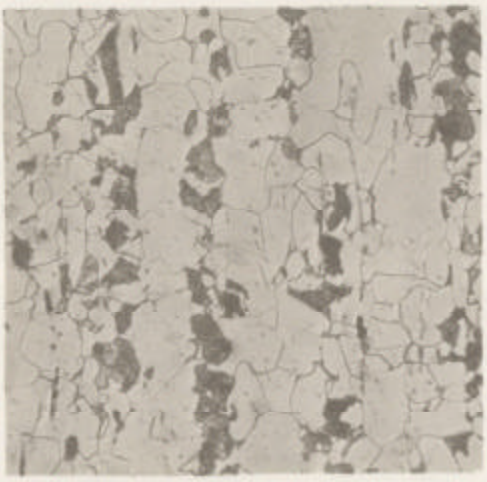

Nital Etch X200

Longitudinal Section

Fig.18 Metallographic Structure of Material Tested

other of a longitudinal section. Both sections were taken from the gage length of one test specimen. The linearized distribution of pearlite due to the hot rolling operation may be seen in the photomicrograph of the longitudinal section.

The hardness of ten test specimens, selected at random, was measured using a standard Rockwell hardness tester. Four hardness measurements were made on each specimen. The average hardnesses of the ten specimens ranged from 47 R_B to 59 R_B. The maximum range of the hardness in any single specimen was 3 R_B.

The surface finish of ten specimens, selected at random, was measured by means of a Brush Surface Analyser. The measurements ranged from 8 micro-inches r.m.s. to 13 micro-inches r.m.s. The maximum depth of scratches ranged from 90 to 130 micro-inches.

VI. TEST PROCEDURE

A. Static Tests

From two to four static tests were made at each of the temperatures at which rapid load tests were made. Stepwise loading was used. Approximately two minutes were allowed to elapse between adjacent test points. The setting of the testing machine was made at the beginning of the interval and the readings were taken at the end. Approximately 10 points were taken in the elastic range, and from 10 to 60 points were taken in the range of plastic deformations up to 5 per cent total strain. Two tests at room temperature were continued until failure occurred. At other temperatures the tests were stopped at 5 per cent strain because of the limited allowable extension of the metal bellows used in the heat exchanger.

The temperature of the specimen could not be maintained within as narrow a range in some of the static tests as it could be in the rapid load tests. For the static tests made at elevated temperatures the specimen temperature varied about $10^{\circ}F$ during a given test. At room temperature and low temperatures the specimen could be maintained within $2^{\circ}F$ of a given temperature throughout the test.

B. Rapid Load Tests

All the rapid load tests reported in this investigation were made using "free loading". This means that the cam of the actuating mechanism of the testing machine was moved at a sufficiently high rate so that the motion of the actuating

piston was not controlled by the cam. Thus the loading was of the form shown by the experimental curves in Fig. 11. The time required to reach full load is independent of the magnitude of the load and is about 7 millisec as shown in Fig. 11. Tests similar to those shown in Fig. 11 were made at various times during the course of the investigation. Such tests always gave essentially the same results, indicating that the damping of the machine remained substantially constant.

The stresses at which the tests were made were chosen to obtain a reasonably uniform distribution of the test points in the plot of delay time vs. stress. At any given temperature, the upper limit of the stress employed was taken to be that stress at which the delay time was about 5 millisec. The reason for this is that, at delay times shorter than about 5 millisec, the test cannot be considered to be performed at constant stress; because an appreciable portion of the time, during which the stress exceeds the static upper yield stress, elapses while the stress is increasing.

The lower limit of the stress employed was taken as that stress at which the delay time was about 10 sec, except in the case of tests made at -75°F. In the latter case the tests were extended to a delay time of 100 sec. The purpose of this was to establish a feature of the test results which extended into the range of delay times from 10 to 100 sec. The sweep generators incorporated in the recording unit were not capable of producing sweep times longer than 10 sec. Therefore the measurements of delay times longer than 10 sec were made with a stop watch. The sweep circuit and the

blanking circuit for the oscilloscope used to record the extensometer were disconnected. Thus the spot of the electron beam of the cathode ray tube was visible at all times, and experienced no motion along the time axis. When the load was applied to the test specimen the spot could be observed to move a short distance along the deformation axis, corresponding to the elastic deformation of the specimen. The stop watch was started at this time. The spot then remained stationary until plastic deformation began. At that time the spot began to move relatively rapidly along the deformation axis, and the watch was stopped. The stop watch was graduated in divisions of 0.1 sec, and the delay time was measured to that accuracy. The stress was measured in the usual manner using an oscilloscope sweep time of 10 sec. It is assumed that the stress remained unchanged for times longer than 10 sec.

A complete series of tests was made at each of four temperatures, -75°F, 73°F, 150°F, and 250°F. For the tests made at -75°F the temperature of the specimen could be adjusted to within ±2°F of the desired temperature by controlling the amount of coolant flowing through the specimen heat exchanger. Once adjusted, the temperature remained constant over long periods of time. However, in the case of the tests made at elevated temperatures this was not true. As has been mentioned previously, the temperature hunted over a range of about 7°F, due to the characteristics of the automatic temperature controller in the oil heating and circulating unit and to the thermal inertia of the system. Nevertheless, the period of this temperature variation (about 10 min) was long

enough so that all the rapid load tests could be made at a temperature within $3^{\circ}F$ or less of the desired temperature. This was accomplished by performing the tests at the proper time in the temperature fluctuation cycle. No special precautions were taken to control the specimen temperature for the tests made at room temperature ($73^{\circ}F$). However, the ambient temperature in the laboratory was quite stable, and did not vary more than $3^{\circ}F$ from $73^{\circ}F$ during the tests.

VII. EXPERIMENTAL RESULTS

A. Static Tension Tests

The principal results of the static tension tests are given in Table I for all the temperatures employed in this investigation. The stress-strain curves up to a total strain of 5 per cent are given in the following figures:

-75°F.....Fig. 19,

75°F.....Fig. 20,

150°F.....Fig. 21,

250°F.....Fig. 22.

Two stress-strain curves up to failure, determined at room temperature, are given in Fig. 23.

B. Rapid Load Tests

The results of the rapid load tests are given in the following tables:

-75°F.....Table II,

73°F.....Table III,

150°F.....Table IV,

250°F.....Table V.

The values of delay time are given to the number of significant figures appropriate for each individual measurement. A final digit 5 in the delay time indicates an accuracy of ± 5 in that place. All other digits in the last place indicate an accuracy of ± 1 in that place. A tracing of a typical record (specimen number 63 tested at -74.5°F) is given in Fig. 16.

TABLE I

RESULTS OF STATIC TENSION TESTS

Specimen Number	Temperature Degrees F	Upper Yield Stress, 10^3 lb/in.^{2}	Lower Yield Stress, 10^3 lb/in.^{2}	Yield Strain Per Cent
4	-75	51.5	40.0	3.5
95	-75	44.6	39.5	3.0
96	-75	43.9	38.0	3.1
		Average 46.7	Average 39.2	Average 3.2
1	69	35.3	29.5	1.7
164	74	41.0	32.4	1.9
165	75	41.8	32.5	2.0
		Average 39.4	Average 31.5	Average 1.9
158	143 to 153	31.6	27.0	1.4
159	144 to 154	39.7	30.7	1.6
161	148 to 159	36.8	27.9	1.5
		Average 36.0	Average 28.5	Average 1.5
162	248 to 255	32.5	29.2	---
163	249 to 255	36.7	27.0	---
		Average 34.6	Average 28.1	

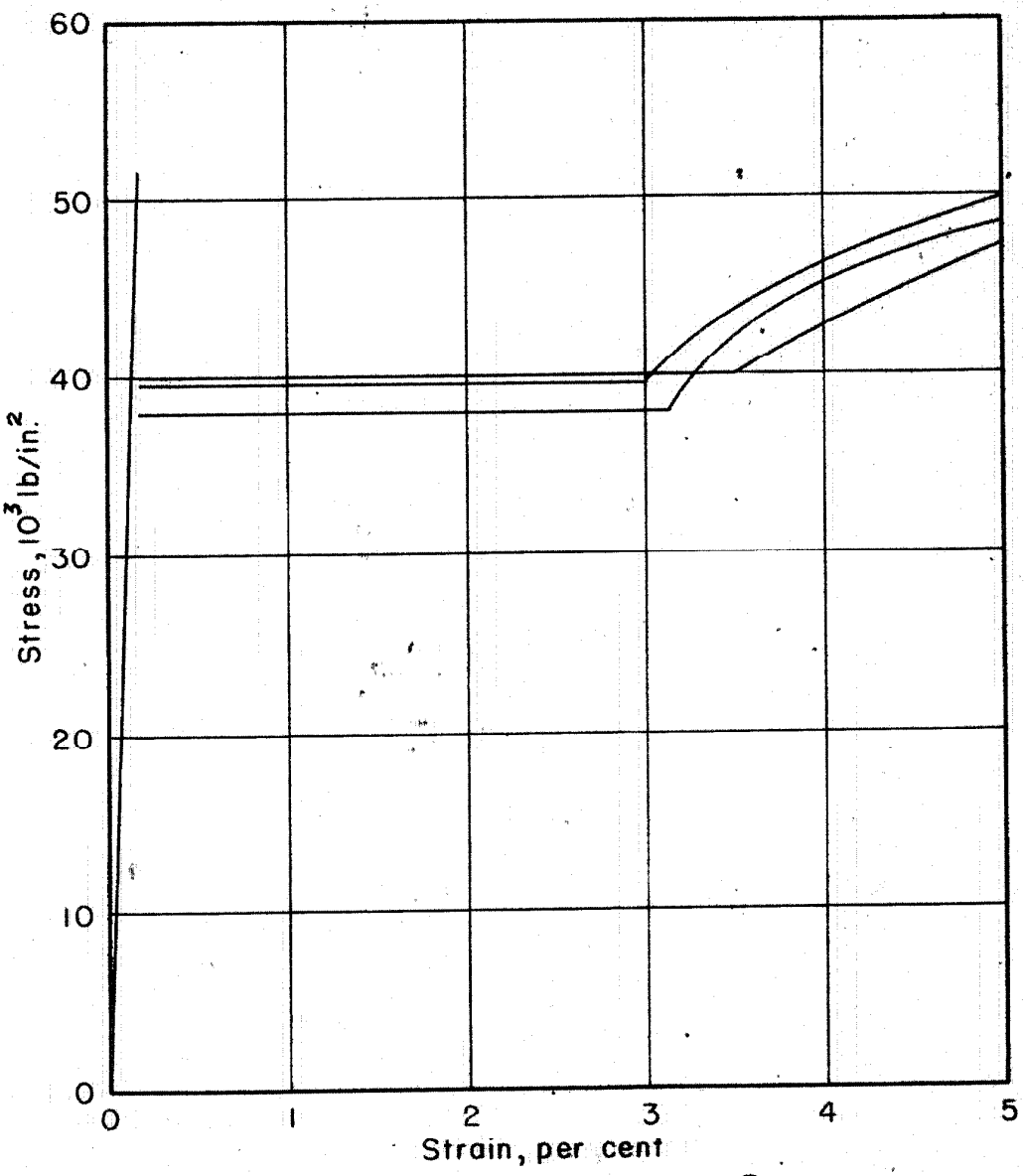

Fig.19 Static Stress vs Strain, −75°F

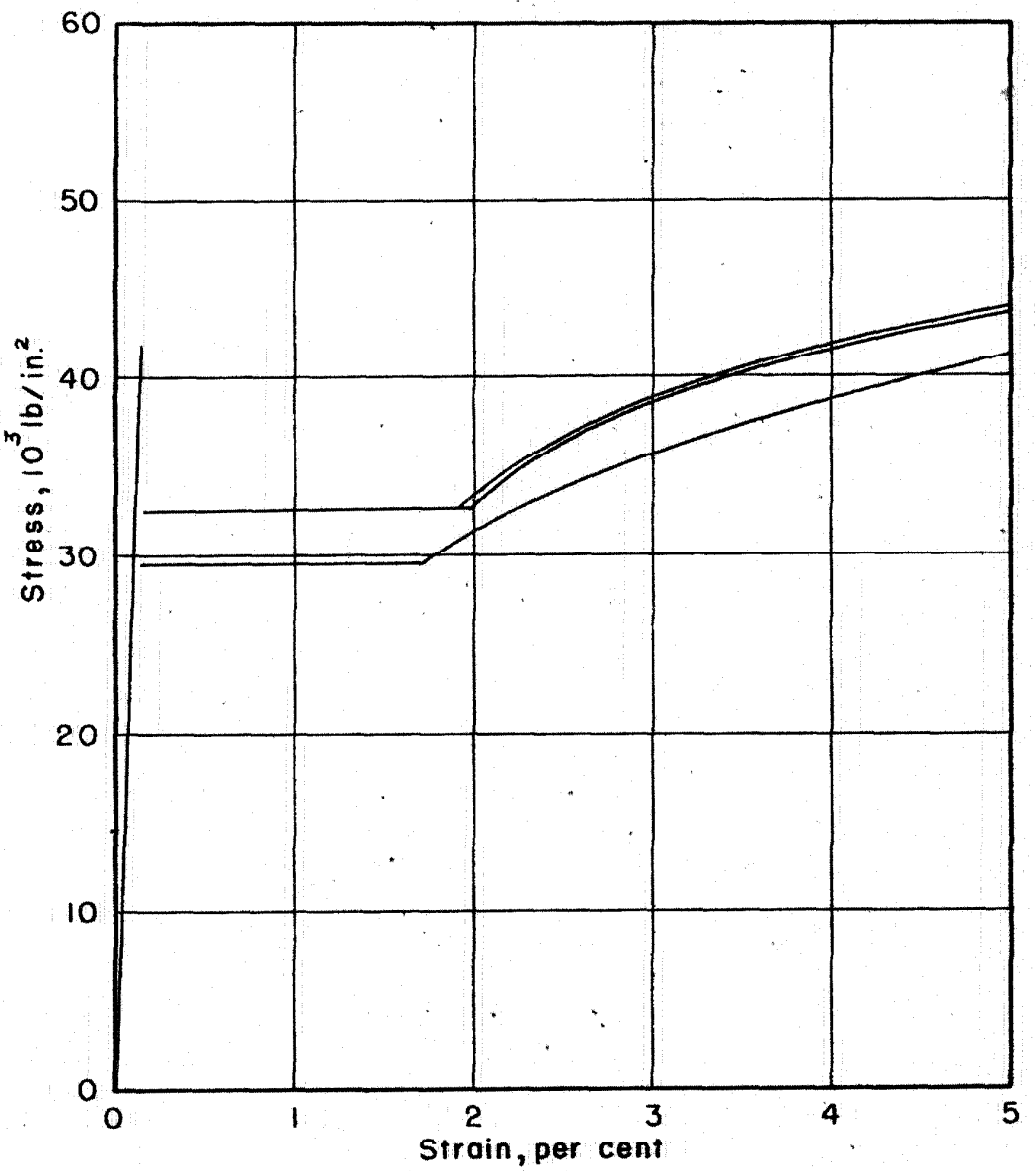

Fig.20 Static Stress vs Strain, +73° F

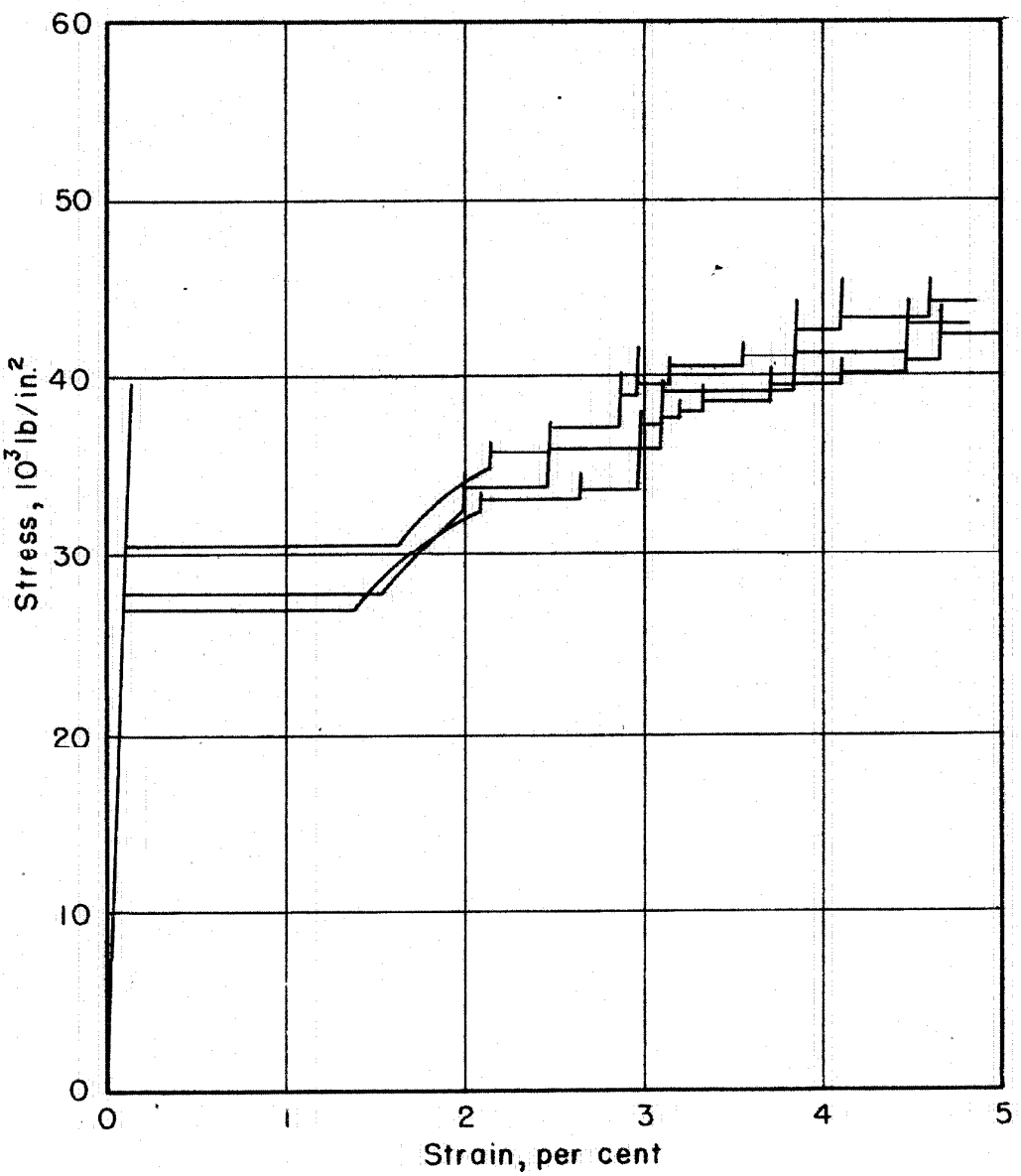

Fig. 21 Static Stress vs Strain, +150° F

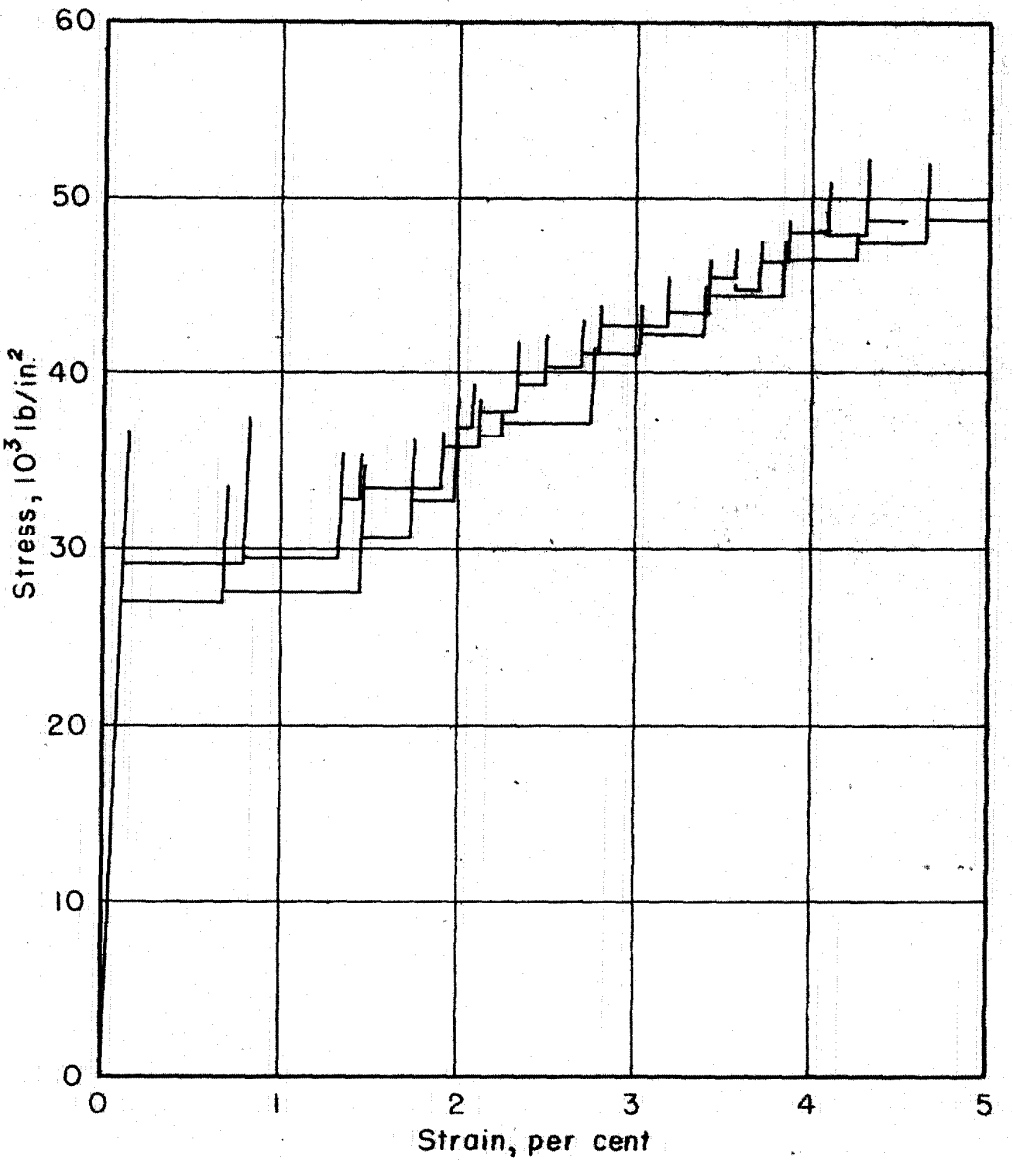

Fig.22 Static Stress vs Strain, +250 °F

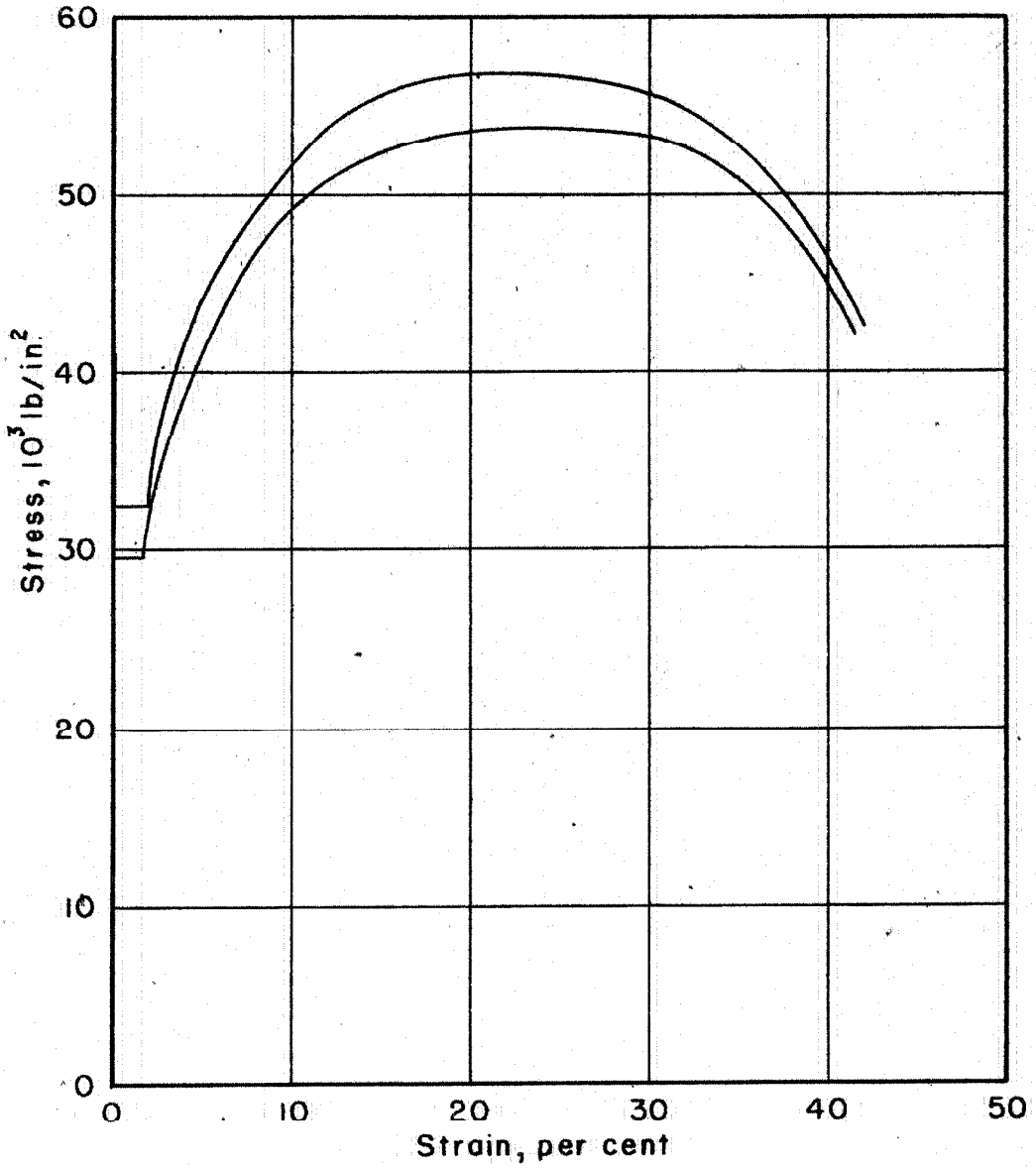

Fig.23 Static Stress vs Strain to Failure at Room Temperature

TABLE II

RESULTS OF RAPID LOAD TESTS AT -75°F

Specimen Number	Temperature Degrees F	Stress 10^3 lb/in.^{2}	Delay Time Sec.
48	-76	68.7	0.03
49	-76	71.5	0.059
50	-74.5	71.8	0.021
51	-77	70.5	0.011
52	-76.5	66.8	0.125
54	-75.5	64.8	0.165
55	-74.5	62.7	0.145
56	-75	63.7	0.325
57	-74.5	60.1	0.185
58	-75.5	59.5	0.82
59	-75.5	70.3	0.0205
60	-76	72.8	0.0245
61	-75	73.7	0.014
63	-74.5	65.2	0.064
64	-75.5	65.2	0.094
65	-75	55.7	0.70
66	-75.5	52.8	1.7
67	-75.5	52.0	6.2
68	-76	55.0	2.8
69	-74.5	52.8	4.7
70	-75	54.5	4.5
71	-75	51.0	6.4
72	-75.5	72.8	0.016
73	-74	74.9	0.0105
74	-76	75.5	0.0120
75	-74.5	72.0	0.030
76	-74.5	49.8	> 30.0
77	-75	52.0	4.8
78	-75.5	51.1	5.6
79	-75	49.5	17.0
80	-75.5	50.1	8.8
81	-75.5	49.8	55.0
82	-75.5	49.8	6.0
83	-75	48.8	7.2
84	-75	46.7	65.0
85	-75	46.3	28.0
86	-75	47.0	> 300.0
87	-75	48.8	6.7
88	-75	47.7	62.0
89	-75.5	47.3	28.0
90	-75	48.2	12.0
92	-75.5	76.2	0.0083

TABLE III

RESULTS OF RAPID LOAD TESTS AT 73°F

Specimen Number	Temperature Degrees F	Stress 10^3 lb/in.^{2}	Delay Time Sec.
9	70	57.7	0.0045
10	70	52.3	0.027
11	71	49.9	0.052
14	71	48.8	0.205
15	72	44.9	0.26
17	72	44.1	0.285
19	72	46.0	0.097
20	75	55.9	0.011
21	75	56.1	0.006
22	75	51.9	0.012
23	75	49.9	0.027
24	74	49.1	0.197
25	75	48.8	0.058
26	74	41.1	0.51
27	72	41.9	0.21
28	73	41.5	0.44
30	74	39.0	> 9.5
31	74	40.9	> 9.5
32	74	40.7	0.35
33	74	40.4	> 9.4
34	74	41.8	4.45
35	74	41.0	> 9.4
36	74	41.8	1.35
37	74	41.0	0.9
38	74	41.3	0.26
39	73.5	41.0	> 9.9
40	74.5	41.5	0.45
44	75	44.5	0.14
45	75	48.3	0.175
46	76	47.4	0.038
47	76	51.3	0.0375

TABLE IV

RESULTS OF RAPID LOAD TESTS AT 150°F

Specimen Number	Temperature Degrees F	Stress 10^3 lb/in.^{2}	Delay Time Sec.
117	148.5	49.6	0.0065
120	151	46.0	0.005
121	151	44.7	0.0045
122	150	44.1	0.0245
123	150	43.0	0.0155
124	150	44.2	> 0.10
125	151	43.5	0.067
126	148	40.4	0.069
127	150	40.7	> 0.30
128	150	40.7	0.012
129	150	39.6	0.27
131	150	39.7	> 1.0
136	152	45.1	0.011
137	150	44.5	0.08
138	151	44.0	0.007
139	150	44.5	0.006
140	151	42.8	> 0.20
141	151	43.5	0.014
142	150	43.2	0.012
143	151	43.0	0.014
144	150	43.0	> 15.0
145	150	41.5	0.015
146	151	39.9	0.010
147	151	40.6	> 0.50
148	151	38.2	0.035
150	150	38.7	0.080
151	151	38.0	0.135
152	152	37.3	0.055
153	151	37.8	> 1.0
154	151.5	44.8	0.0045
157	151.5	43.6	0.0055

TABLE V

RESULTS OF RAPID LOAD TESTS AT 250°F

Specimen Number	Temperature Degrees F	Stress 10^3 lb/in.^{2}	Delay Time Sec.
97	247	38.8	< 0.005
98	249	40.3	0.005
100	253	38.3	0.060
102	252	39.2	> 0.160
103	253	40.5	0.150
104	250	40.0	0.022
105	251	43.3	< 0.005
106	252	39.8	0.021
107	250	41.0	< 0.005
108	251	40.2	0.010
110	250	38.0	> 60.0
111	250	40.0	< 0.005
112	250	39.5	> 30.0
113	251	40.7	< 0.005
114	250	39.7	< 0.005

All of the rapid load test results are plotted in Fig. 24, which shows the relation between delay time (on a logarithmic scale) and stress, at the four test temperatures. The lines drawn in the figure to represent the data are determined as follows. It is assumed that the experimental results, for any given temperature, may be represented by two intersecting straight lines on the semi-log plot. The first is a line of constant stress and the second a line of negative slope, as shown in Fig. 24. The experimental points are divided into two groups, each group being associated with one of the two lines. The line of constant stress represents the data for all delay times greater than the delay time at which the two lines intersect. The sloping line represents the data for all shorter delay times. The line of constant stress is taken to be the line representing the mean stress of all the associated points.

The line of negative slope is determined so that the sum of the squares of the orthogonal deviations of the experimental points from the line is a minimum. This is done in the following manner. Let

$$y = \log t,$$

where t is the delay time. Then the line is of the form

$$y = a - b\sigma, \qquad (1)$$

where σ is the stress, and a and b are constants to be determined in such a way as to minimize the sum of the squares of the orthogonal deviations. The orthogonal deviation, x_i, of the i'th experimental point is given by

$$x_i = [y_i - (a - b\sigma_i)] \frac{1}{\sqrt{1+b^2}};$$

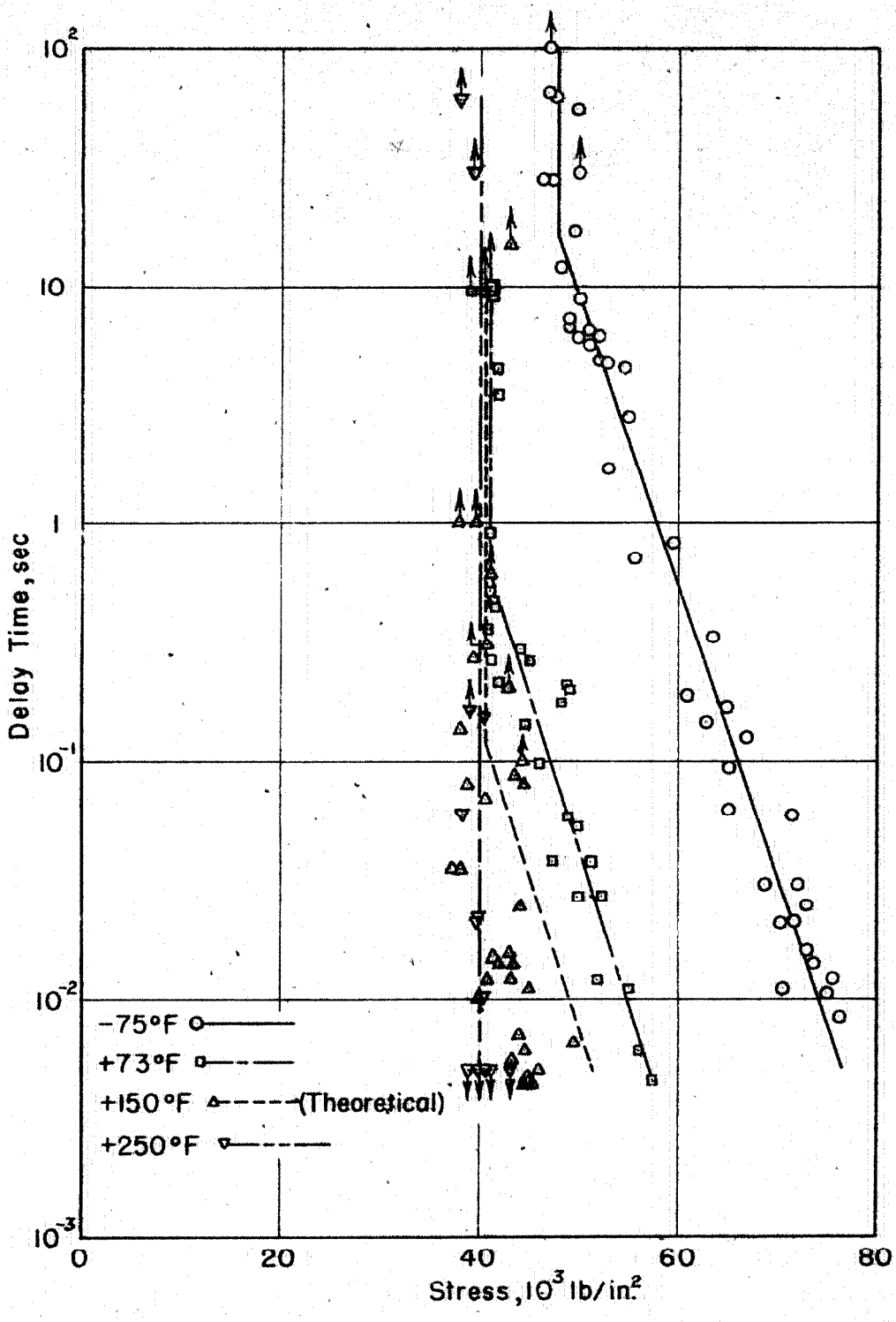

Fig.24 Delay Time for the Initiation of Plastic Deformation as a Function of Stress

and the sum of the squares of these deviations is

$$\sum_{i=1}^{n} x_i^2 = \frac{1}{(1+b^2)} \sum_{i=1}^{n} \left[y_i - (a - b\sigma_i) \right]^2, \qquad (2)$$

where n is the number of experimental points.

To minimize (2) the partial derivatives with respect to the two parameters, a and b, are set equal to zero:

$$\frac{\partial}{\partial a} \left(\sum_{i=1}^{n} x_i^2 \right) = 0,$$

$$\frac{\partial}{\partial b} \left(\sum_{i=1}^{n} x_i^2 \right) = 0.$$

This leads to

$$\sum_{i=1}^{n} y_i - na + b \sum_{i=1}^{n} \sigma_i = 0, \qquad (3)$$

and

$$(1+b^2) \sum_{i=1}^{n} \sigma_i \left[y_i - (a - b\sigma_i) \right] - b \sum_{i=1}^{n} \left[y_i - (a - b\sigma_i) \right]^2 = 0. \qquad (4)$$

Using (3) to eliminate a from (4) and rearranging, the following quadratic in b is obtained:

$$b^2 \left[\frac{1}{n} \left(\sum_{i=1}^{n} \sigma_i \right) \left(\sum_{i=1}^{n} y_i \right) - \sum_{i=1}^{n} \sigma_i y_i \right]$$

$$+ b \left[\sum_{i=1}^{n} \sigma_i^2 - \sum_{i=1}^{n} y_i^2 - \frac{1}{n} \left(\sum_{i=1}^{n} \sigma_i \right)^2 + \frac{1}{n} \left(\sum_{i=1}^{n} y_i \right)^2 \right]$$

$$+ \sum_{i=1}^{n} \sigma_i y_i - \frac{1}{n} \left(\sum_{i=1}^{n} \sigma_i \right) \left(\sum_{i=1}^{n} y_i \right) = 0. \qquad (5)$$

The coefficients of b in (5) are computed numerically from the experimental data and the equation is solved for b. One root gives the slope of the desired line. The other leads to a maximum of the sum of the squares of the orthogonal deviations, and is discarded. After computing the slope, b, the intercept, a, is readily found by the use of (3).

For representation of these lines by empirical equations it is convenient to change the form of the constants, a and b. Let $a = \log t_o$, and $b = \frac{1}{\sigma_o}$,

then equation (1) may be written in the form

$$t = t_o e^{-\frac{\sigma}{\sigma_o}}. \qquad (6)$$

This is more satisfactory from a dimensional point of view than equation (1). Also let the line of constant stress be represented by $\sigma = \bar{\sigma}$.

The numerical values of the empirical constants, t_o, σ_o, and $\bar{\sigma}$, are given in Table VI. The values of t_o and σ_o cannot be determined for the tests made at 150°F and 250°F because the data does not extend to small enough values of the delay time, as can be seen in Fig. 24. The sloping dashed line in Fig. 24, associated with the tests made at 150°F, represents a theoretical extrapolation from the results at -75°F and 73°F. The construction of this line is discussed later.

TABLE VI

EMPIRICAL CONSTANTS TO FIT THE RELATIONS $t = t_o e^{-\frac{\sigma}{\sigma_o}}$ AND $\sigma = \bar{\sigma}$ TO THE EXPERIMENTAL DATA

Temperature Degrees F	t_o sec	σ_o 10^3 lb/in.^{2}	$\bar{\sigma}$ 10^3 lb/in.^{2}
-75	11.9×10^6	3.54	47.8
73	13.1×10^4	3.35	41.0
150	———	———	40.7
250	———	———	40.0

VIII. DISCUSSION OF RESULTS

The form of the records of load and extension vs. time obtained in rapid load tests, as shown in Fig. 16, has been explained by Professor D. S. Clark and the author (17) in the following manner. After the load has been applied, the specimen behaves essentially elastically for a well defined delay time, as shown by the first horizontal portion of the extension-time record. At the end of the delay time plastic deformation begins rather abruptly, and proceeds at an approximately constant rate. The drop in load which takes place when plastic deformation begins corresponds to the drop of the beam in a static test. As in static tests, the magnitude of the drop in load is due to the combined effects of the material and the characteristics of the testing machine. In the rapid load tests, the motion of the fluid in the machine, during the period of rapid plastic deformation, causes a pressure rise across the damping tubes. This raises the fluid pressure below the loading piston. Thus the load acting upon the specimen is decreased. The drop in load is proportional to the rate of plastic deformation. The load which the specimen will sustain is also a function of the rate of plastic deformation. Therefore, the rate of plastic deformation takes on that value at which the load which the specimen will sustain is equal to the applied load.

The fact that the initial plastic deformation proceeds at a constant rate may be explained by the inhomogeneous nature

of the yielding in annealed low carbon steel. It is known (15) that, to a first approximation, the full yield strain appears initially at one or more points of stress concentration in a tension specimen. With continued stretching, the boundaries of the plastically deformed regions progress through the specimen until the entire gage length is occupied by the yield strain. At that point the cold hardening region of the stress-strain curve is reached, and subsequent plastic deformation occurs uniformly over the gage length of the specimen. Therefore, it is reasonable to assume that the period of constant rate of plastic deformation, observed in rapid load tests, is a consequence of the propagation of one or more yield strain fronts along the gage length of the specimen.

In the record shown in Fig. 16, the period of constant plastic deformation rate is abruptly terminated, and no further strain occurs. This is simply because the actuating piston of the rapid load testing machine reached the limit of its travel. It can be seen that a second drop in load occurs at that point. This represents the stress relaxation of the specimen when plastic deformation is suddenly terminated. The record in Fig. 16 shows that the limit of travel of the machine was reached before the yield strain had progressed over the entire gage length of the specimen.

In some tests the yield strain is completed before the limit of travel of the machine is reached. In this case the rate of plastic deformation is observed to decrease progressively after the yield strain is completed. This occurs in the cold hardening range of the stress-strain curve. The

stress-strain relation followed in rapid load tests differs considerably from the static stress-strain relation, for annealed low carbon steel. It has been shown (17) that both the yield strain and the strain hardening portion of the stress-strain relation take place at increased stresses in the rapid load tests. This result is in agreement with results obtained by Miklowitz (15). The effect of these phenomena upon the propagation of plastic deformation waves in longitudinal impact has been discussed by White (25), in an analysis of the experimental results of Duwez and Clark (8).

The primary results of this investigation are the experimental data, obtained at several temperatures, relating the delay time for the initiation of plastic deformation to the applied stress. These data are shown in Fig. 24. They show that there exists a critical stress, $\bar{\sigma}$, for each temperature, at which the behavior of annealed low carbon steel changes markedly. The lines drawn in the figure were determined by the arbitrary procedure outlined previously. The transition between the two modes of behavior may not be as sharp as these lines indicate. However, it may be seen from an examination of the experimental points that the transition is quite abrupt.

Previous results of tests performed at room temperature, which are reported by Professor D.S. Clark and the author (17), do not exhibit an abrupt transition in the delay time-stress relation. There are several possible explanations for this discrepancy. First, different steels were used in

the two investigations. The transition point for the steel used in the earlier work may occur at a delay time greater than 10 sec, which was the upper limit of the delay times investigated. Second, the specimens used in the first experiments were machined, by turning in a lathe, after the material had been annealed; and they were not re-annealed after machining. The cold worked surface produced by this procedure may have influenced the behavior of the material. Finally, the number of experimental points obtained in the earlier experiments may not have been sufficient to define the transition adequately, due to the scatter of the points.

The static tension tests were included in this investigation for the purpose of providing a comparison with the rapid load test results. Since the curves of delay time vs. stress, shown in Fig. 24, exhibit a constant lower limiting stress, $\overline{\sigma}$, it is reasonable to suppose that $\overline{\sigma}$ is the true static upper yield stress of the material. If the values of the static upper yield stress given in Table I are compared with the values of $\overline{\sigma}$ given in Table VI, it is seen that at -75°F and 73°F the average values of the static upper yield stress are equal to $\overline{\sigma}$, within the experimental scatter. However, at 150°F and 250°F the static upper yield stresses are appreciably lower than $\overline{\sigma}$.

The scatter of the measured values of the static upper yield stress is considerably greater than the scatter in stress of the rapid load test points corresponding to the critical stress, $\overline{\sigma}$. The experimental errors in the static tests are less than in the rapid load tests, and the scatter in the

static upper yield stress is greater than the probable experimental error. Therefore, it may be concluded that at stresses near the limit of elasticity of the material, defects in the test specimens may cause yielding after rather long periods of time, whereas the initiation of yielding is less sensitive to defects during shorter periods of time. The defects may consist of surface irregularities, non-metallic inclusions, exceptional variations in grain size, and other microscopic and submicroscopic structural variations in the material.

The static stress-strain relations at 150°F and 250°F, shown in Fig. 21 and Fig. 22 respectively, show clearly the phenomenon of strain ageing. At these temperatures appreciable strain ageing takes place in the interval between readings of the load and extension during the static test. This interval was approximately 2 min. The secondary yield points appear in the curves for 150°F after the strain has reached the strain hardening range. At 250°F they appear within the range of the yield strain. During the performance of these tests it was noted, in several instances, that the secondary yield points exhibit a definite delay time for the resumption of plastic deformation.

The slopes of the lines of Fig. 24 representing the relation between delay time and stress, at stresses above the critical stress and for the temperatures of -75°F and 73°F, are equal within the scatter of the data. This is shown by the values of the constant σ_0, given in Table VI. From this result, it might be assumed that the mechanism associated with the delay time phenomenon is a thermally activated process,

in which the delay time and temperature, at constant stress, are related by a function of the form

$$t \propto e^{\frac{Q}{RT}}, \qquad (1)$$

where T is the absolute temperature, R the gas constant, and Q the activation energy. Since the slopes of the lines in Fig. 24 are approximately equal, the activation energy is almost independent of stress. From the experimental data the activation energy is computed to be

Q = 8,000 calorie/mole, or 0.35 electron volt/atom, at a stress of 50,000 lb/in.^{2}

By setting the proportionality factor in equation (1) equal to the stress function previously given to represent the data at a constant temperature, namely $e^{-\sigma/\sigma_o}$, all the data at -75°F and 73°F may be represented by a single relation of the form

$$t = \bar{t}\, e^{-\sigma/\sigma_o}\, e^{\frac{Q}{RT}}, \qquad (2)$$

for stresses greater than the critical stresses, $\bar{\sigma}$. The value of the new constant, $\bar{t}$, is computed to be

$$\bar{t} = 0.10 \text{ sec},$$

and σ_o may be taken as the average of the values given for the two temperatures in Table VI, namely

$$\sigma_o = 3.45 \times 10^3 \text{ lb/in.}^2$$

Using the value 2.0 cal/mole degree C for R, equation (2) becomes

$$t = 0.10\, e^{-\frac{\sigma}{3450}}\, e^{\frac{4000}{T}}, \qquad (3)$$

where t is the delay time in seconds, σ the stress in pounds per square inch, and T the absolute temperature in degrees Kelvin.

If equation (3) is valid, it should be possible to predict the test results obtained at other temperatures. However, it is found that the test results at 150°F do not fit this relation. The dotted line in Fig. 24 represents results predicted by equation (3) for 150 F. The discrepancy is greater than the experimental scatter. At a given stress, the experimental delay time is less than predicted.

The results of this investigation may also be compared with the dislocation theory of yielding in low carbon steel, given by Cottrell and Bilby (21), which has been discussed previously. The portion of the saturated carbon "atmosphere" around a dislocation which exerts the primary influence upon the motion of the dislocation consists of a row of carbon atoms parallel to the dislocation. There is one carbon atom per atomic plane in the direction of the dislocation. The row of carbon atoms lies in the plane which passes through the center of the dislocation and is perpendicular to the slip plane. For a positive dislocation the carbon atoms lie below the slip plane because that is the region of greatest dilatation in the dislocation field.

The interaction energy between the dislocation and the associated row of carbon atoms is calculated with the aid of the relation for the stresses in a dislocation field which has been given by Koehler (26). If an external stress is applied to the material, the dislocation moves in the direction of the slip plane, with respect to the carbon atoms. The interaction energy is calculated as a function of the distance through which the dislocation has moved. The applied stress required

to move the dislocation through this distance is taken to be proportional to the gradient of the interaction energy. The relations found for the interaction energy and the stress as functions of the distance through which the dislocation has moved are:

$$V(x) = -\frac{A}{\rho}\,\frac{1}{\{1+(x/\rho)^2\}}\,,$$

and

$$\frac{\sigma(x)}{\sigma_m} = \frac{16}{3\sqrt{3}}\,\frac{(x/\rho)}{\{1+(x/\rho)^2\}^2}\,;$$

where x is the distance the dislocation moves, measured from the equilibrium position,

ρ is the distance between the equilibrium position of the dislocation and the row of carbon atoms,

σ_m is the maximum value reached by the stress,

and A is a constant, which depends upon the elastic constants of iron and the lattice expansion produced by a carbon atom.

These two relations are shown in graphical form in Fig. 25.

By considering the effect of thermal fluctuations upon the stress required to separate the dislocation from its "atmosphere", an expression for the activation energy for the separation process is derived. Referring to Fig. 25, if an external stress, σ_1/σ_m, is applied, the dislocation moves to the position x_1/ρ. If the dislocation remains straight, the activation energy for the release of the dislocation by thermal fluctuations is

$$V(x_2/\rho) - V(x_1/\rho)$$

minus the work done by the external stress when the dislocation moves from x_1/ρ to x_2/ρ. It is found that this energy

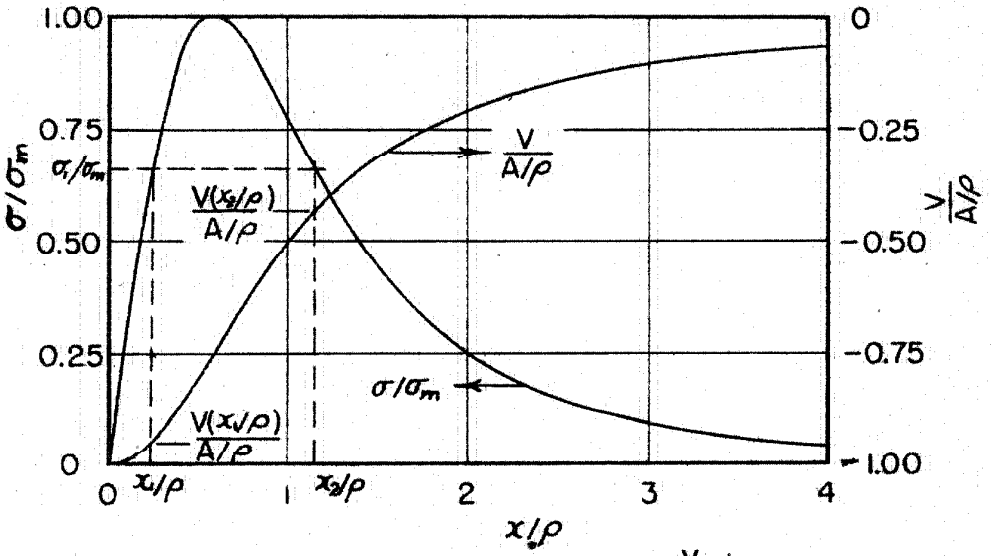

Fig.25 Stress, σ/σ_m, and Interaction Energy, $\frac{V}{A/\rho}$, as Functions of the Displacement, x/ρ, of a Dislocation (Cottrell and Bilby)

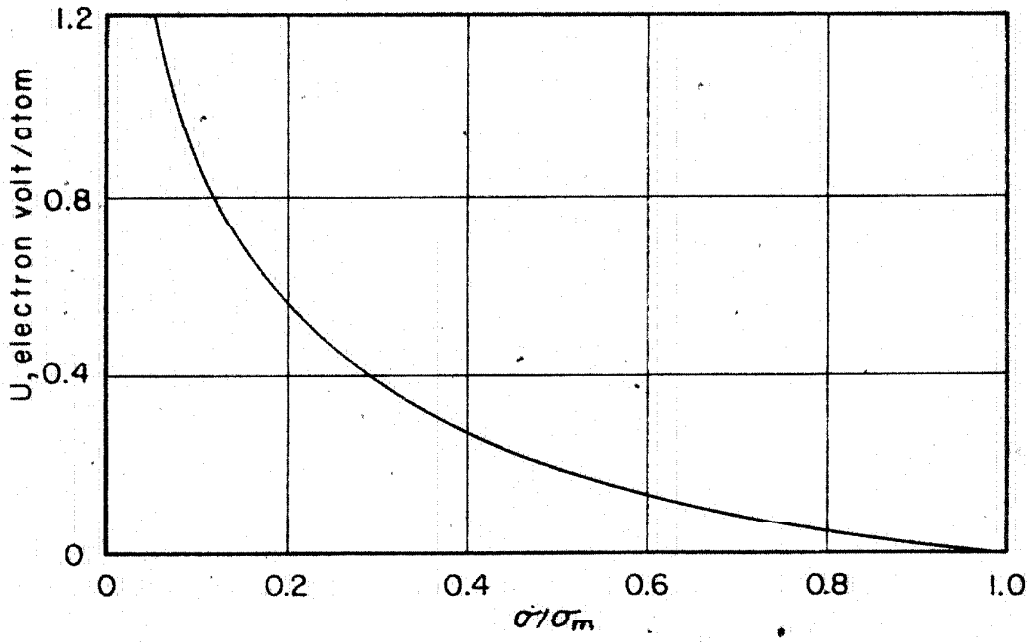

Fig.26 Activation Energy, U, to Separate a Dislocation From Its "Atmosphere" as a Function of Applied Stress, σ/σ_m (Cottrell and Bilby)

is quite large. Therefore, it is assumed that the dislocation is distorted, so that a relatively small portion of it moves beyond the position x_2/ρ. If the distorted portion of the dislocation is initially large enough it will progressively extend along the dislocation, finally causing complete separation. This mechanism introduces an additional term into the activation energy, which is the energy required to increase the length of the dislocation, in order to form the local distortion. To compute this term, it is assumed that the dislocation behaves like a one dimensional soap film, having an energy W per unit length.

The final result obtained for the activation energy required for separation of a dislocation from its "atmosphere" of carbon atoms is

$$U(\sigma/\sigma_m) = D(\sigma/\sigma_m)\left[AE(\sigma/\sigma_m)\left\{2W\rho - AE(\sigma/\sigma_m)\right\}\right]^{\frac{1}{2}}, \qquad (4)$$

where $$D(\sigma/\sigma_m) = \frac{x_2}{\rho} - \frac{x_1}{\rho},$$

and $$E(\sigma/\sigma_m) = \frac{2}{\left\{1+\left(\frac{x_1}{\rho}\right)^2\right\}} - \frac{2}{\left(\frac{x_2}{\rho} - \frac{x_1}{\rho}\right)}\left\{\tan^{-1}\left(\frac{x_2}{\rho}\right) - \tan^{-1}\left(\frac{x_1}{\rho}\right)\right\} - \frac{3\sqrt{3}}{8}\left(\frac{x_2}{\rho} - \frac{x_1}{\rho}\right)\frac{\sigma}{\sigma_m}.$$

The activation energy, $U(\sigma/\sigma_m)$, has been computed, and is shown in Fig. 26. The various constants were given the following values, which were considered to be the most probable values by Cottrell and Bilby:

$A = 3 \times 10^{-21}$ erg cm/atomic plane,

$W = 1$ electron volt/atomic plane,

and $\rho = 2\text{Å}$.

The mean time required to separate a dislocation from its "atmosphere" is proportional to $e^{U/kT}$,

where k is Boltzmann's constant.

If a mechanism relating the motion of dislocations with the initiation of macroscopically observable plastic deformation is assumed, then the above result, obtained by Cottrell and Bilby, may be applied to a description of the results of the present investigation. A very simple assumption is that plastic deformation begins after a certain number of dislocations have separated from their "atmosphere" within a prescribed volume of the material. Furthermore, if it is assumed that this number of separated dislocations is large enough so that the total time required to reach this number is statistically well defined, then the delay time for the initiation of plastic deformation is given by

$$t = t' e^{U/kT}, \qquad (5)$$

where t' is a constant which is independent of both stress and temperature.

The relation given by equation (5) may be fitted to the experimental data given in Fig. 24 at two points, by a suitable choice of the constants t' and σ_m. The points at which the fit was made were chosen to be the points at a stress of 50,000 lb/in.^{2} for the temperatures -75°F and 73°F. The numerical values obtained for the constants are

$$t' = 4.85 \times 10^{-8} \text{ sec},$$

and $\sigma_m = 155{,}000$ lb/in.^{2};

and the curves are shown in Fig. 27, where they are compared with the experimental data.

The slopes of the theoretical lines could be brought into closer agreement with the experimental results by a

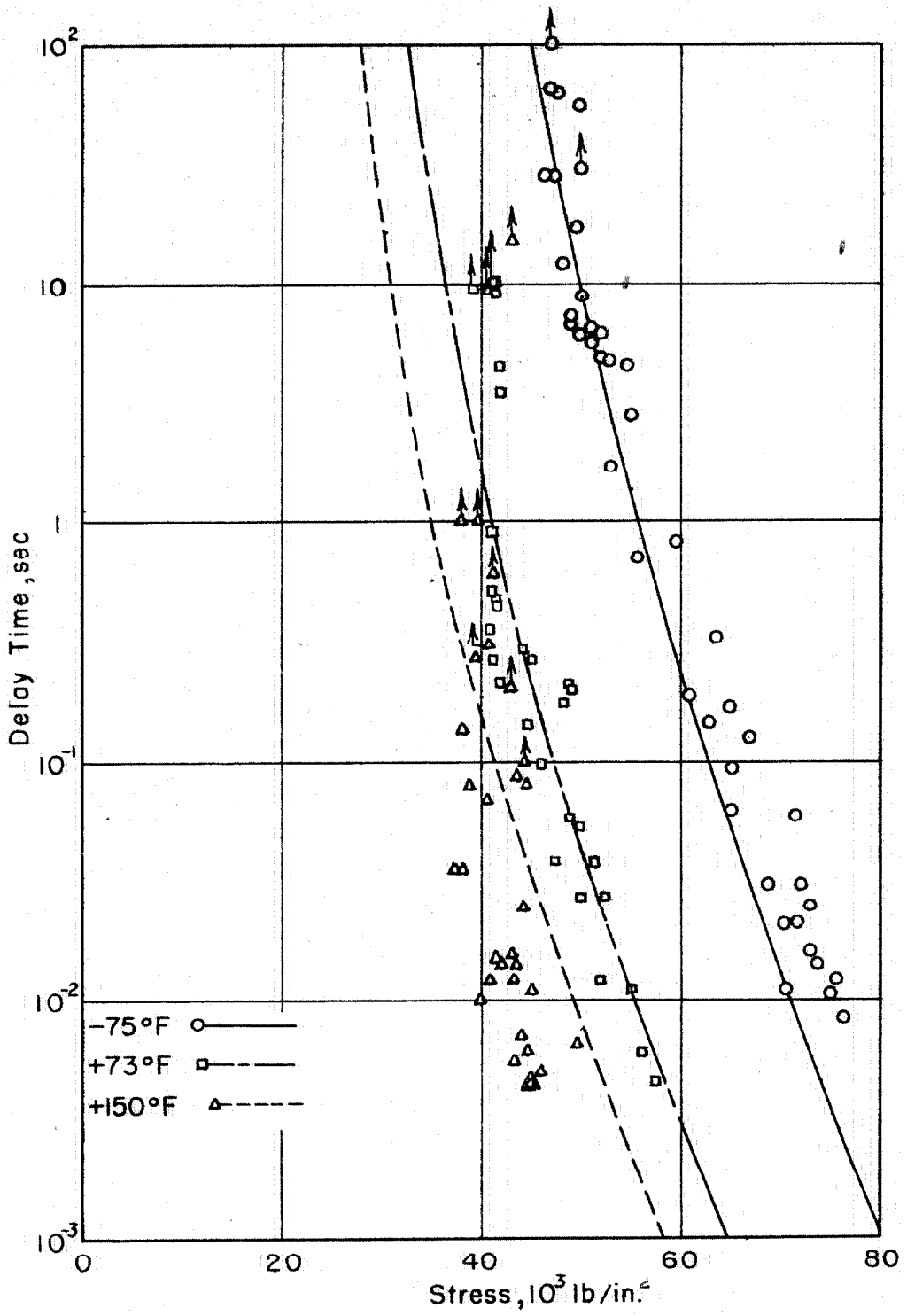

Fig.27 Comparison of Experimental and Theoretical Delay Time vs. Stress Relations

suitable adjustment of the constants, A, V, and ρ , which appear in the expression for the activation energy. However, the theory does not account for constant stress portion of the experimental results, given by the critical stress $\overline{\sigma}$. Also it does not agree with the experimental results obtained at 150°F. The latter discrepancy is of the same type as that found for the expression which wasused in the first attempt to fit the data.

Some additions and modifications of the theory which might provide for closer agreement with experiment may be postulated. The assumption that macroscopic plastic deformation occurs after a certain number of dislocations have been separated from their "atmospheres" of carbon atoms is probably too crude. To obtain an adequate description of the experimental results it is necessary to know the mechanism by which moving dislocations initiate plastic deformation. Some recent experimental results reported by A. N. Holden and J. H. Hollomon (27) indicate that this mechanism involves the polycrystaline nature of the material. Holden and Hollomon performed experiments similar to those of Low and Gensamer (20), but on single iron crystals rather than on polycrystaline specimens. They found that the introduction of carbon and nitrogen into single crystals of iron did not cause a yield point to occur in the stress-strain curve, whereas Low and Gensamer showed that carbon and nitrogen do cause a yield point in polycrystaline iron. The theory of Cottrell and Bilby does not depend upon the grain size of the material. So, if this theory is assumed to be essentially correct, an

additional theory, involving the polycrystaline nature of the material and relating the motion of dislocations to macroscopic plastic deformation, is necessary for an adequate description of the experimental results.

Such a theory could account for the critical stress, $\bar{\sigma}$, observed in the experimental delay time-stress relations. However, it probably would not account for the thermal dependence of the sloping portion of the delay time-stress curves. It has been shown that both the simple relation first suggested and the theory of Cottrell and Bilby exhibit essentially the same discrepancy in predicting the thermal dependence of the delay time. This suggests that the form of the relation

$$t \propto e^{Q/RT},$$

used in both cases, is in error.

The relation given above is based upon the assumption that the particles of the system obey the Maxwell-Boltzmann statistics. It may be seen that this assumption is not quite correct by considering the results of the Debye theory for the specific heats of solids. The Debye characteristic temperature, Θ, is that temperature below which the ability of the oscillators constituting the solid to change their energies by arbitrary amounts begins to be restricted by the quantum conditions imposed upon their energies. Thus, at temperatures less than Θ, the probability for a thermal fluctuation which is able to separate a dislocation from its "atmosphere" within a given time decreases more rapidly with decreasing temperature than is given by the relation $e^{-Q/RT}$.

Therefore the mean time to separate a dislocation at low temperatures is greater in relation to the mean time at high temperatures than would be predicted by the relation

$$t \propto e^{Q/RT}.$$

This is the trend observed in the experimental results in this investigation.

The Debye characteristic temperature for iron is $\Theta = 420^{\circ}K$(28). The ratios of the absolute temperatures employed in this investigation to the characteristic temperature are then as follows:

Temperature °F	$\frac{T}{\Theta}$
-75	0.51
73	0.70
150	0.80
250	0.94

Therefore it is reasonable to suppose that the considerations discussed above have an effect upon the experimental results reported.

In this investigation, the minimum temperature employed ($-75^{\circ}F$) was limited by the nature of the temperature control equipment. However, additional tests at still lower temperatures, such as the temperature of liquid air, would be necessary to define the deviations of the temperature dependence of the delay time from the $e^{Q/RT}$ law adequately. At temperatures greater than about $150^{\circ}F$, the sloping portion of the delay time-stress curve occurs at delay times which are too small to be investigated with the present rapid load testing machine, because the time for the rise of load in the

machine (7 millisec) is too great. A machine of the same general type could probably be constructed which would have a rise time of one or two milliseconds by employing higher air and fluid pressures. In this way the size of the moving parts and the quantity of fluid in the machine would be decreased, thus reducing the equivalent mass of the system. Hence, a shorter rise time would be obtained. However, the minimum rise time which could be reached in this way, without oscillation of stress in the specimen, is limited by the time required for pressure waves to traverse the air and fluid chambers of the machine. Tests in which the delay time is less than about one millisecond might be made by the method of the longitudinal impact of long bars.

IX. SUMMARY AND CONCLUSIONS

From the results of this investigation, it may be concluded that a rather well defined critical stress exists for annealed low carbon steel, below which the delay time for the initiation of plastic deformation increases much more rapidly with decreasing stress than at stresses exceeding the critical stress.

The experimental results show that the temperature dependence of the delay time at stresses above the critical stress cannot be adequately represented by a classical thermal activation function of the form

$$t \propto e^{Q/RT}.$$

It is also shown that the dislocation theory of yielding in low carbon steel, which has been given by Cottrell and Bilby, does not account for the existence of the critical stress observed in the delay time-stress relations.

In order to account for the discrepancies between the experimental results and existing theory, two concepts are suggested which might lead to closer agreement. The first is that a mechanism which describes the manner in which dislocations initiate macroscopic plastic deformation is required, and that this mechanism involves the polycrystaline nature of the material. The second is that, in the temperature range below the Debye characteristic temperature for the material, deviations from the Maxwell-Boltzmann statistics should be considered in order to describe the thermal dependence of the

delay time for the initiation of plastic deformation in annealed low carbon steel.

REFERENCES

(1) H.C.Mann, "High Velocity Tension Impact Tests," Proceedings, Am. Soc. Testing Mats. (1936), Vol. 36, Part II, p. 65.

(2) D. S. Clark and G. Datwyler, "Stress-Strain Relations under Tension Impact Loading," Proceedings, Am. Soc. Testing Mats. (1938), Vol. 38, Part II, p. 98.

(3) M. Manjoine and A. Nadai, "High Speed Tension Tests at Elevated Temperatures," Proceedings, Am. Soc. Testing Mats. (1940), Vol. 40, p. 822; Transactions, Am. Soc. Mechanical Engrs., Journal of Applied Mechanics (1941), Vol. 8, No. 2, p. A-77.

(4) A. V. DeForest, C. W. MacGregor, and A. R. Anderson, "Rapid Tension Tests Using the Two-Load Method," Am. Inst. Mining and Metallurgical Engrs., Metals Technology (December 1941), p. 1.

(5) E. R. Parker and C. Ferguson, "The Effect of Strain Rate upon the Tensile Impact Strength of Some Metals," Transactions, Am. Soc. Metals (1942), Vol. 30, p. 68.

REFERENCES (continued)

(6) D. S. Clark, "The Influence of Impact Velocity on the Tensile Characteristics of Some Aircraft Metals and Alloys," Nat. Advisory Comm. Aeronautics (October 1942), Technical Note No. 868.

(7) D. S. Clark and P. E. Duwez, "Discussion of the Forces Acting in Tension Impact Tests of Materials," Transactions, Am. Soc. Mechanical Engrs., Journal of Applied Mechanics (1948), Vol. 15, No. 3, p. A-243.

(8) P. E. Duwez and D. S. Clark, "An Experimental Study of the Propagation of Plastic Deformation under Conditions of Longitudinal Impact," Proceedings, Am. Soc. Testing Mats. (1947), Vol. 47, p. 502.

(9) Theodore von Kármán, "On the Propagation of Plastic Deformation in Solids," National Defense Research Committee (February 2, 1942), Report No. A-29.

(10) Theodore von Kármán and P. E. Duwez, "On the Propagation of Plastic Strain in Solids," Presented at the Sixth International Congress for Applied Mechanics, September 1946, Paris.

REFERENCES (continued)

(11) C. F. Elam, "The Influence of Rate of Deformation on the Tensile Test with Special Reference to the Yield Point in Iron and Steel," Proceedings, Roy. Soc. of London (1938), Vol. 165, p. 568.

(12) E. A. Davis, "The Effect of the Speed of Stretching and the Rate of Loading on the Yielding of Mild Steel," Transactions, Am. Soc. Mechanical Engrs., Journal of Applied Mechanics (1938), Vol. 60, p. A-137.

(13) J. Winlock and R. W. E. Leiter, "Some Factors Affecting the Plastic Deformation of Sheet and Strip Steel and Their Relation to Deep Drawing Properties," Transactions, Am. Soc. Metals (1937), Vol. 25, p. 163.

(14) J. Winlock and R. W. E. Leiter, "Some Observations on the Yield Point of Low-Carbon Steel," Transactions, Am. Soc. Mechanical Engrs. (1939), Vol. 61, p. 581.

(15) J. Miklowitz, "The Initiation and Propagation of the Plastic Zone in a Tension Bar of Mild Steel as Influenced by the Speed of Stretching and Rigidity of Testing Machine," Transactions, Am. Soc. Mechanical Engrs., Journal of Applied Mechanics (1947), Vol. 14, No. 1, p. A-31.

REFERENCES (continued)

(16) Bertram Hopkinson, "Effects of Momentary Stresses in Metals," Proceedings, Roy. Soc. of London (1905), Vol. 74, p. 498.

(17) D. S. Clark and D. S. Wood, "The Time Delay for the Initiation of Plastic Deformation at Rapidly Applied Constant Stress," to be presented at the meeting of the Am. Soc. for Testing Mats. in June 1949, and to be published.

(18) C. A. Edwards, D. L. Phillips, and H. W. Jones, Journal Iron and Steel Inst. (1940), Vol. 142, p. 199.

(19) J. L. Snoek, "Effect of Small Quantities of Carbon and Nitrogen on the Elastic and Plastic Properties of Iron," Physica (1941), Vol. 8, p. 711.

(20) J. R. Low, Jr., and M. Gensamer, "Aging and the Yield Point in Steel," Transactions, Am. Inst. of Mining and Metallurgical Engrs. (1944), Vol. 158, p. 207.

(21) A. H. Cottrell and B. A. Bilby, "Dislocation Theory of Yielding and Strain Ageing of Iron," Proceedings, Physical Society of London (1949), Sec. A, Vol. 62, Part 1, p. 49.

REFERENCES (continued)

(22) D. S. Wood and D. S. Clark, "The Design and Construction of a Hydro-Pneumatic Machine for Rapid Load Tensile Testing," Report No. I submitted to U. S. Air Force, Air Materiel Command, 21 May 1947.

(23) David Arthur Elmer, "The Influence of Low Temperature on the Tensile Impact Properties of Two Shipbuilding Steels," thesis, California Institute of Technology (1948).

(24) Max M. Frocht, "Factors of Stress Concentration Photoelastically Determined," Transactions, Am. Soc. Mechanical Engrs., Journal of Applied Mechanics (1935), Vol. 57, p. A-67.

(25) M. P. White, "On the Impact Behavior of a Material with a Yield Point," Transactions, Am. Soc. Mechanical Engrs., Journal of Applied Mechanics (1948), Vol. 16, No. 1, p. 39.

(26) J. S. Koehler, "On the Dislocation Theory of Plastic Deformation," Phys. Rev. (1941), Vol. 60, p. 397.

(27) A. N. Holden and J. H. Hollomon,""Homogeneous Yielding of Carburized and Nitrided Single Iron Crystals," Am. Inst. Mining and Metallurgical Engrs., Journal of Metals (February 1949), Vol. 1, No. 2, p. 179.

REFERENCES (continued)

(28) F. Seitz, "The Physics of Metals," McGraw-Hill Book Co., Inc., New York (1943), p. 59.